

# Simulating the Real World: A Unified Survey of Multimodal Generative Models

Yuqi Hu\*, Longguang Wang\*, Xian Liu\*, Ling-Hao Chen\*, Yuwei Guo\*, Yukai Shi\*, Ce Liu\*, Anyi Rao, Zeyu Wang, and Hui Xiong<sup>†</sup>, *Fellow, IEEE*

**Abstract**—Understanding and replicating the real world is a critical challenge in Artificial General Intelligence (AGI) research. To achieve this, many existing approaches, such as world models, aim to capture the fundamental principles governing the physical world, enabling more accurate simulations and meaningful interactions. However, current methods often treat different modalities, including 2D (images), videos, 3D, and 4D representations, as independent domains, overlooking their interdependencies. Additionally, these methods typically focus on isolated dimensions of reality without systematically integrating their connections. In this survey, we present a unified survey for multimodal generative models that investigate the progression of data dimensionality in real-world simulation. Specifically, this survey starts from 2D generation ([appearance](#)), then moves to video ([appearance+dynamics](#)) and 3D generation ([appearance+ geometry](#)), and finally culminates in 4D generation that integrate all dimensions. To the best of our knowledge, this is the first attempt to systematically unify the study of 2D, video, 3D and 4D generation within a single framework. To guide future research, we provide a comprehensive review of datasets, evaluation metrics and future directions, and fostering insights for newcomers. This survey serves as a bridge to advance the study of multimodal generative models and real-world simulation within a unified framework.

**Index Terms**—Generative models, image generation, video generation, 3D generation, 4D generation, deep learning, literature survey.

## 1 INTRODUCTION

For decades, the research community has aspired to develop systems that encapsulate the fundamental principles of the physical world, a cornerstone in the journey towards Artificial General Intelligence (AGI) [1]. Central to this endeavor is simulating the real world with machines, aiming to capture the complexities of reality through the lens of multimodal generative models. The resultant world simulator holds the promise of advancing the understanding of real world, unlocking transformative applications such as virtual reality [2], games [3], robotics [4] and autonomous driving [5].

The term “world simulator” was first introduced by Ha David [6], drawing an analogy to the concept of a mental model [7] in cognitive science. Building on this perspective, modern researches [8] formulate the simulator as an abstract framework that enables intelligent systems to simulate the real world through multimodal generative models. These

models encode visual contents and spatial-temporal dynamics of the real world into compact representations. As geometry, appearance, and dynamics jointly contribute to the realness of generated contents, these three aspects are widely investigated by the community [9]. Traditional real-world simulation methods have long relied on graphics techniques that incorporate geometry, texture, and dynamics. Specifically, geometry and texture modeling [10] are employed to create the objects while methods like keyframe animation [11] and physics-based simulation [12] are adopted to simulate the movement and behavior of objects over time.

Despite great progress, these traditional methods often require extensive manual designs, heuristic rule definitions, and computationally expensive processing, limiting their scalability and adaptability to diverse scenarios. Recently, learning-based approaches, particularly multimodal generative models, have revolutionized content creation by providing a data-driven approach to realistic simulations. These approaches reduce the reliance on manual efforts, improve generalization across tasks, and enable intuitive interactions between human and models. For example, Sora [13] has garnered significant attention for its realistic simulation capabilities, demonstrating an early-stage understanding of physical laws. The emergence of such generative models introduces new perspectives and methodologies, addressing the limitations of traditional methods by reducing the need for extensive manual design and computationally expensive modeling while enhancing adaptability and scalability in diverse simulation scenarios.

Though existing generative models offer powerful techniques for synthesizing realistic content in distinct data dimensions, the real world exhibits inherently high-dimensional complexity, and a comprehensive review that systematically integrates these advancements across differ-

- Yuqi Hu, Zeyu Wang, and Hui Xiong are with the Thrust of Artificial Intelligence, The Hong Kong University of Science and Technology (Guangzhou), Guangzhou 511458, China. E-mail: yhu873@connect.hkust-gz.edu.cn, zeyuwang@ust.hk, xionghui@ust.hk.
- Anyi Rao is with the Division of Arts and Machine Creativity, The Hong Kong University of Science and Technology, Hong Kong, China. E-mail: anyirao@ust.hk.
- Longguang Wang is with the School of Electronics and Communication Engineering, Shenzhen Campus of Sun Yat-sen University, Sun Yat-sen University, Shenzhen, 518107, China. E-mail: wanglg9@mail.sysu.edu.cn.
- Xian Liu and Yuwei Guo are with The Chinese University of Hong Kong, Hong Kong, China. E-mail: alvinliu@ie.cuhk.edu.hk, guoyw@ie.cuhk.edu.hk.
- Ling-Hao Chen and Yukai Shi are with Tsinghua University, Guangdong, 518000, China. E-mail: evan@lhchen.top, shiyk22@mails.tsinghua.edu.cn.
- Ce Liu is with Shanghai Academy of AI for Science, Shanghai, China. E-mail: celiu0901@gmail.com

\* Equal contribution. <sup>†</sup> Corresponding author: Hui Xiong.

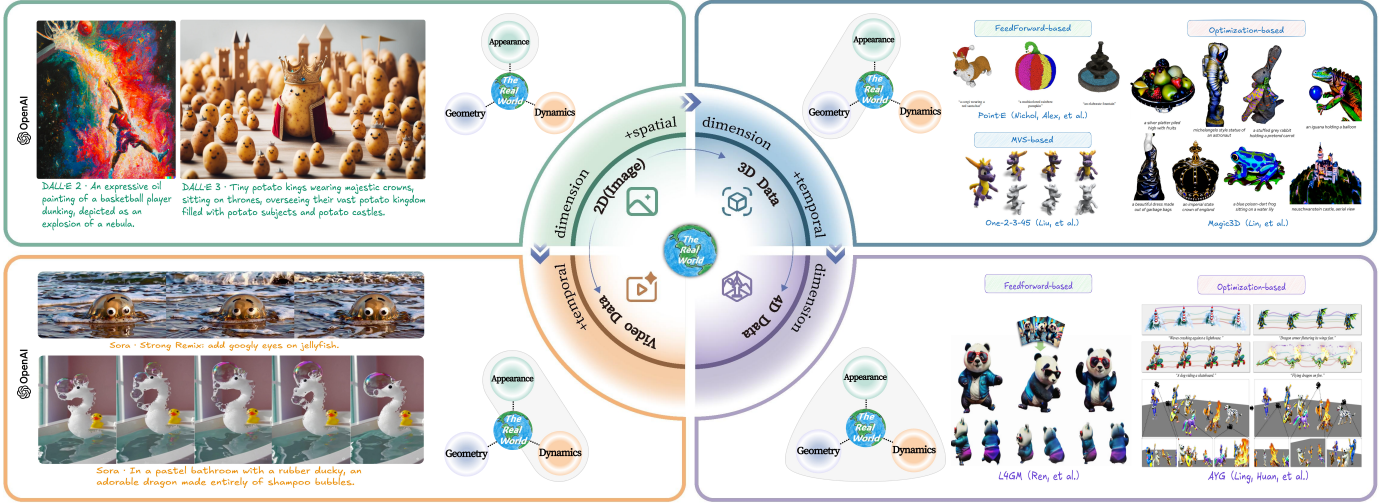


Fig. 1: Roadmap of dimensional growth from 2D images to video, 3D, and 4D content in real-world simulation, outlining a conceptual taxonomy based on the coverage of data properties (i.e., appearance, geometry, and dynamics).

ent dimensions is still absent. This survey aims to bridge this gap by unifying the study of real-world simulation through from the perspective of data dimension growth, as illustrated in Figure 1. Specifically, we start from 2D generation (appearance only) and then extend it to video and 3D generation by incorporating dynamics and geometry dimensions, respectively. Finally, we culminates in 4D generation by integrating all dimensions.

In summary, this survey makes three key contributions. *First*, it provides a systematic review of methods for real world simulation from the perspective of data dimension growth through the lens of multimodal generative models. To the best of our knowledge, this is the first survey that unifies the study of 2D, video, 3D, and 4D generation, offering a structured and comprehensive overview of this research area. *Second*, it surveys the commonly used datasets, their properties, and the corresponding evaluation metrics from various perspectives. *Third*, it identifies open research challenges, aiming to provide guidance for further exploration in this field.

We envision this survey as a resource that provides valuable insights for newcomers and fosters critical analysis among experienced researchers. The survey is organized as follows. Section 2 introduces the foundational concepts of deep generative models. Section 3 presents four key paradigms: 2D, video, 3D, and 4D generation. Section 4 reviews datasets and evaluation metrics for these paradigms. Finally, Section 5 outlines future directions, and Section 6 concludes the survey.

## 2 PRELIMINARIES

Deep generative models learn complicated and high-dimensional data distribution with the aid of deep neural networks. Denote the data sample as  $\mathbf{x}$  and its distribution as  $p_{data}(\mathbf{x})$ , the objective of deep generative models is to approximate the  $p_{data}(\mathbf{x})$  with  $p_{\theta}(\mathbf{x})$ , where  $\theta$  is the parameter of models. In this section, we briefly review several mainstream generative models (Table 1), including generative adversarial networks (GANs) [14], variational autoencoders (VAEs) [15], autoregressive models (AR Models) [16], normalizing flows (NFs) [17], and diffusion models [18].

TABLE 1: Comparison of deep generative models.

Model Types	Advantages	Disadvantages
GANs [14]	Flexible	Unstable training
VAEs [15]	Data compression	1) Posterior collapse 2) Blur
AR Models [16]	Explicit density	1) Markov assumption 2) Difficult to parallelize
NFs [17]	Explicit density	Limited capacity
Diffusion Models [18]	High-quality samples	Expensive computation

### 2.1 Generative Adversarial Networks (GANs)

GANs avoid the parametric form of  $p_{\theta}(\mathbf{x})$  but represent  $p_{\theta}(\mathbf{x})$  as the distribution of samples produced by a generator. It has been shown that  $p_{\theta}(\mathbf{x})$  will converge to  $p_{data}(\mathbf{x})$  under certain conditions [14].

Specifically, the generator takes a noise vector  $\mathbf{z}$  as input to synthesize a data sample  $G(\mathbf{z}; \theta_g)$ . The  $p_{\theta}(\mathbf{x})$  is defined as the distribution of  $G(\mathbf{z}; \theta_g)$ , where  $\mathbf{z} \sim p_{\mathbf{z}}(\mathbf{z})$ . Meanwhile, the discriminator  $D(\mathbf{x}; \theta_d)$  identifies whether an input data sample is a real one or a synthetic one. During training, the discriminator is trained to distinguish the generated samples from real data, while the generator is trained to deceive the discriminator. The process can be formulated as:

$$\min_G \max_D V(G, D) = \mathbb{E}_{\mathbf{x} \sim p_{data}(\mathbf{x})} [\log D(\mathbf{x}; \theta_d)] + \mathbb{E}_{\mathbf{z} \sim p_{\mathbf{z}}(\mathbf{z})} [\log(1 - D(G(\mathbf{z}; \theta_g); \theta_d))]. \quad (1)$$

### 2.2 Variational Autoencoders (VAEs)

The variational autoencoders (VAEs) formulate the  $p_{\theta}(\mathbf{x})$  as,

$$p_{\theta}(\mathbf{x}) = \int p_{\theta}(\mathbf{x}|\mathbf{z})p_{\theta}(\mathbf{z})d\mathbf{z}, \quad (2)$$

where  $p(\mathbf{z})$  is a prior distribution of  $\mathbf{z}$ , and  $p_{\theta}(\mathbf{x}|\mathbf{z})$  is the distribution of  $\mathbf{x}$  conditioned on  $\mathbf{z}$ . However, since this integration is usually intractable, VAEs maximize the lower bound of  $\log p_{\theta}(\mathbf{x}) \geq -\text{KL}(q_{\theta}(\mathbf{z}|\mathbf{x})||p_{\theta}(\mathbf{z})) + \mathbb{E}_{q_{\theta}(\mathbf{z}|\mathbf{x})} [\log p_{\theta}(\mathbf{x}|\mathbf{z})]$ , where  $\text{KL}(q_{\theta}(\mathbf{z}|\mathbf{x})||p_{\theta}(\mathbf{z}))$  is the KL divergence between  $q_{\theta}(\mathbf{z}|\mathbf{x})$  and  $p_{\theta}(\mathbf{z})$ , and  $\mathbb{E}_{q_{\theta}(\mathbf{z}|\mathbf{x})} [\log p_{\theta}(\mathbf{x}|\mathbf{z})]$  is computed by the Stochastic Gradient Variational Bayes estimator [15].

### 2.3 Autoregressive Models (AR Models)

Autoregressive Models (AR) models factorize  $p_\theta(\mathbf{x})$  as the product of conditional probabilities to alleviate the difficulty of modeling multivariate joint probability,

$$p_\theta(\mathbf{x}) = p(x_1, \dots, x_d) = \prod_{i=1}^d p_\theta(x_i | x_1, \dots, x_{i-1}), \quad (3)$$

where  $d$  is the sequence length.

Recently, numerous efforts have been made to employ AR models to model pixels in an image sequentially [19]–[21].

### 2.4 Normalizing Flows (NFs)

NFs employ an invertible neural network  $g(\cdot)$  to map  $\mathbf{z}$  from a known and tractable distribution to the real data distribution. In this way,  $p_\theta(\mathbf{x})$  can be formulated as,

$$p_\theta(\mathbf{x}) = p(f(\mathbf{x})) |\det J(g(g^{-1}(\mathbf{x})))|^{-1}, \quad (4)$$

where  $g^{-1}(\cdot)$  is the inverse of  $g(\cdot)$ , and  $J(g(\mathbf{z})) = \frac{\partial g}{\partial \mathbf{z}}$  is the Jacobian of  $\mathbf{g}$ . NFs construct arbitrarily complicated non-linear invertible functions by compositing a set of  $N$  bijective functions and define  $g = g_N \circ \dots \circ g_1$ .

### 2.5 Diffusion Models

Diffusion models are a class of probabilistic generative models that iteratively corrupt data by introducing noise and subsequently learn to reverse this process to generate samples. We define  $p_\theta(\mathbf{x})$  with an energy term  $s_\theta(\mathbf{x})$ ,

$$p_\theta(\mathbf{x}) = \exp(-s_\theta(\mathbf{x})) / Z_\theta, \quad (5)$$

where  $Z_\theta = \int \exp(-s_\theta(\mathbf{x})) d\mathbf{x}$  is the normalization term.

Since  $Z_\theta$  is intractable to compute, the diffusion models learn the score function  $\nabla_{\mathbf{x}} \log p_\theta(\mathbf{x}) = -\nabla_{\mathbf{x}} s_\theta(\mathbf{x})$  instead.

The forward process that transforms data distribution to standard Gaussian is defined by  $d\mathbf{x} = f(\mathbf{x}, t)dt + g(t)d\mathbf{w}$ , where  $f(\mathbf{x}, t)$  is the drift coefficient,  $g(t)$  is the diffusion coefficient,  $\mathbf{w}$  is the standard Wiener process, and  $t \in [0, 1]$ . The samples are generated by the corresponding reverse process, which is described by  $d\mathbf{x} = [f(\mathbf{x}, t) - g^2(t)\nabla \log p_t(\mathbf{x})]dt + g(t)d\bar{\mathbf{w}}$ , where  $\bar{\mathbf{w}}$  is a standard Wiener process when time flows backward from 1 to 0.

## 3 PARADIGMS

This section presents methods for simulating the real world from the perspective of data dimension growth. It begins with 2D generation (Section 3.1) for appearance modeling and then move to video generation (Section 3.2) and 3D generation (Section 3.3) by incorporating dynamics and geometry dimensions. Finally, by integrating all these three dimensions, recent advances in 4D generation (Section 3.4) are presented.

### 3.1 2D Generation

Recently, significant advancements have been made in the field of generative models, particularly in text-to-image generation. Text-to-image generation has attracted attention for its capability to produce realistic images from textual descriptions by capturing the appearance of the real world. Utilizing techniques like diffusion models, large language models (LLMs), and autoencoders, these models achieve high-quality and semantically accurate image generation.

#### 3.1.1 Algorithms

**Imagen** [22] builds on the principles established by GLIDE but introduces significant optimizations and improvements. Instead of training a task-specific text encoder from scratch, Imagen uses pre-trained and frozen language models and reduces computational demands. Imagen tested models trained on image-text datasets (e.g., CLIP [23]) and models trained on pure text datasets (e.g., BERT [24] and T5 [25]). This practice shows that scaling up language models enhances image fidelity and text congruence more effectively than enlarging image diffusion models.

**DALL-E** [26] (version 1) uses a transformer architecture that processes both text and images as a single stream of data. DALL-E 2 [27] utilizes the powerful semantic and stylistic capabilities of CLIP [23], which employs a generative diffusion decoder to reverse the process of the CLIP image encoder. DALL-E 3 [28] builds upon the advancements of DALL-E 2 [27], offering significant improvements in image fidelity and text alignment. It enhances text understanding, allowing for more accurate and nuanced image generation from complex descriptions. DALL-E 3 is integrated with ChatGPT [29], enabling users to brainstorm and refine prompts directly within the ChatGPT interface, which simplifies the process of generating detailed and tailored prompts. The model produces images with higher realism and better alignment to the provided text, making it a powerful tool for both creative and professional applications.

**DeepFloyd IF** [30] is celebrated for its exceptional photo-realism and advanced language understanding. This system is modular, featuring a static text encoder and three sequential pixel diffusion modules. Initially, the base model creates 64×64 pixel images from textual descriptions. These images are then enhanced to 256×256 pixels and further to 1024×1024 pixels by two super-resolution models. Each phase utilizes a static text encoder derived from the T5 [25] transformer to generate text embeddings, which are subsequently processed by a U-Net architecture with integrated cross-attention and attention pooling mechanisms.

**Stable Diffusion** (SD) [31], also known as Latent Diffusion Model (LDM), enhances training and inference efficiency on limited computational resources while producing high-quality and diverse images. The denoising process takes place in the latent space of pre-trained autoencoders, which map images into a spatial latent space. The underlying U-Net architecture is augmented with a cross-attention mechanism to model the conditional distribution, which can include text prompts, segmentation masks, and more. It used BERT tokenizer [24] as text encoding and trained on the LAION-400M [32] dataset to generate images at a resolution



of  $256 \times 256$  (with a latent resolution of  $32 \times 32$ ). Building on Stable Diffusion, SDXL [33] employs a U-Net backbone that is three times larger. It introduces additional attention blocks and a larger cross-attention context by utilizing a second text encoder. Additionally, SDXL includes a refinement model that enhances the visual fidelity of samples generated by SDXL through a post-hoc image-to-image technique.

**FLUX.1** [34] utilizes a hybrid architecture that integrates multimodal and parallel diffusion transformer blocks, achieving a remarkable scale of 12 billion parameters. By employing flow matching, a straightforward yet effective technique for training generative models, FLUX.1 outperforms prior state-of-the-art diffusion models. The suite also features rotary positional embeddings and parallel attention layers, greatly improving model performance and efficiency.

### 3.2 Video Generation

Text-to-video generation models adapt text-to-image frameworks to handle the additional dimension of dynamics in the real world. We classify these models into three categories based on different generative machine learning architectures. Figure 2 summarizes recent text-to-video generation techniques. For further surveys, readers can refer to more detailed reviews [62], [63] in this subfield.

#### 3.2.1 Algorithms

**(1) VAE- and GAN-based Approaches.** Before diffusion models, video generation research has advanced through two primary approaches: VAE-based and GAN-based methods, each contributing unique solutions to the challenges of video synthesis. VAE-based methods evolved from SV2P [35] in stochastic dynamics to a combination of VQ-VAE [64] with transformers in VideoGPT [65], efficiently handling high-resolution videos through hierarchical discrete latent variables. Notable improvements came from the parameter-efficient architecture in FitVid [36] and the integration of adversarial training for more realistic predictions. Parallel developments in GAN-based approaches brought significant innovations, starting with MoCoGAN [37], which decomposes content and motion components for controlled generation. StyleGAN-V [38] advances this by treating videos as time-continuous signals through positional embeddings, while DIGAN [39] introduces implicit neural representations for improved continuous video modeling. StyleInV [40] leverages a temporal style-modulated inversion network with pre-trained StyleGAN [66] generators, marking another milestone in high-quality frame synthesis with temporal coherence.

**(2) Diffusion-based Approaches.** Text-to-video generation has recently seen significant advancements, with approaches generally falling into two categories: U-Net-based architectures and transformer-based architectures.

**(i) U-Net-based Architectures.** The pioneering Video Diffusion Models (VDM) [41] achieved high-fidelity, temporally coherent video generation by extending image diffusion architectures and introducing joint image-video training for reduced gradient variance. Make-A-Video [42] advanced text-to-video generation without paired text-video data by leveraging existing visual representations [23] and innovative spatial-temporal modules. Imagen

Video [43] introduced a cascade of diffusion models combining base generation with super-resolution, while MagicVideo [44] achieved efficient generation through latent diffusion in low-dimensional space. GEN-1 [45] focused on structure-preserving editing using depth estimates, while PYoCo [46] demonstrated efficient fine-tuning with limited data through carefully designed video noise priors. Align-your-Latents [47] achieved high-resolution generation ( $1280 \times 2048$ ) by extending Stable Diffusion [31] with temporal alignment techniques. Show-1 [67] combined pixel-based and latent-based approaches for enhanced quality and reduced computation. VideoComposer [48] introduced a novel paradigm for controllable synthesis through a Spatio-Temporal Condition encoder, enabling flexible composition based on multiple conditions. AnimateDiff [49] presented a plug-and-play motion module with transferable motion priors and introduced MotionLoRA for efficient adaptation. PixelDance [50] enhanced generation by incorporating both first and last frame image instructions alongside text prompts.

**(ii) Transformer-based Architectures.** Following the success of Diffusion Transformer (DiT) [68], transformer-based models gained prominence. VDT [53] introduced modularized temporal and spatial attention mechanisms for diverse tasks including prediction, interpolation, and completion. W.A.L.T [54] achieved photorealistic generation through a unified latent space and causal encoder architecture, producing high-resolution videos at  $512 \times 896$ . Snap Video [69] improved training efficiency 3.31 times through spatially and temporally redundant pixel handling, while GenIron [55] scaled to over 3B parameters with motion-free guidance. Luminia-T2X [56] integrated multiple modalities through zero-initialized attention and tokenized latent spatial-temporal space. CogVideoX [57] excelled in long-duration video generation through expert transformers, 3D VAEs, and progressive training, achieving state-of-the-art performance validated by multiple metrics. The groundbreaking Sora [13] is an advanced diffusion transformer model that emphasizes generating high-quality images and videos across different resolutions, aspect ratios, and durations. Sora achieves flexible and scalable generation capabilities by tokenizing the latent spatial-temporal space.

**(3) Autoregressive-based Approaches.** Parallel to diffusion-based methods, autoregressive frameworks inspired by large language models (LLMs) have emerged as an alternative approach to video generation. These methods typically follow a two-stage process: first encoding visual content into discrete latent tokens using vector quantized auto-encoders like VQ-GAN [70] and MAGVIT [59], [71]–[74], then modeling the token distribution in the latent space. CogVideo [60], a 9-billion-parameter transformer model built upon the pre-trained text-to-image model CogView [75], represents a significant advancement in this direction. It employs a multi-frame-rate hierarchical training strategy to enhance text-video alignment and, as one of the first open-source large-scale pre-trained text-to-video models, establishes new benchmarks in both machine and human evaluations. VideoPoet [61] introduces a decoder-only transformer architecture for zero-shot video generation, capable of processing multiple input modalities including images, videos,

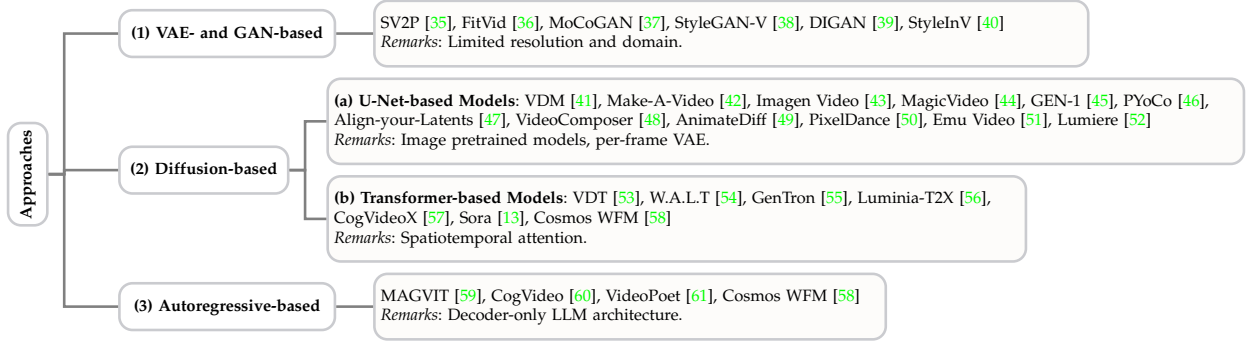


Fig. 2: Overview of text-to-video generation technologies categorized by three main approaches.

text, and audio. Following LLM training paradigms with pretraining and task-specific adaptation stages, VideoPoet achieves state-of-the-art performance in zero-shot video creation, particularly excelling in motion fidelity through its diverse generative pretraining objectives.

### 3.2.2 Applications

**(1) Video editing** has recently benefited significantly from diffusion models, enabling sophisticated modifications while maintaining temporal consistency. The field has evolved through several innovative approaches addressing different aspects of video manipulation. Early developments include Tune-A-Video [76], which pioneered a one-shot tuning paradigm extending text-to-image diffusion models to video generation through spatiotemporal attention mechanisms. Temporal consistency has been addressed through various approaches. VidToMe [77] introduced token merging for aligning frames, while EI [78] developed specialized attention modules. Several works focused on specialized editing capabilities. Ground-A-Video [79] tackled multi-attribute editing through a grounding-guided framework, while Video-P2P [80] introduced cross-attention control for character generation. Recent frameworks like UniEdit [81] and AnyV2V [82] represent the latest evolution, offering tuning-free approaches and simplified editing processes. Specialized applications such as CoDeF [83] and Pix2Video [84] have introduced innovative techniques for temporally consistent processing and progressive change propagation. These methods successfully balance content editing with structural preservation, marking significant advancements in video manipulation technology.

**(2) Novel view synthesis** has been revolutionized by video diffusion models, which benefit from learned priors on real-world geometry, enabling high-quality view generation from limited input images. ViewCrafter [85] pioneered this direction by integrating video diffusion models with point-based 3D representations, introducing iterative synthesis strategies and camera trajectory planning for high-fidelity results from sparse inputs. Camera control has emerged as a crucial aspect, with CameraCtrl [86] introducing precise camera pose control through a plug-and-play module. Several innovative methods have addressed view consistency challenges. ViVid-1-to-3 [87] reformulated novel view synthesis as video generation of camera movement, while NVS-Solver [88] introduced a zero-shot paradigm that modulates diffusion sampling with given views. This trend shows a

convergence toward leveraging video diffusion priors while maintaining geometric consistency and camera control, enabling increasingly realistic synthesis applications.

**(3) Human animation in videos** has gained significance in video generation, which plays a pivotal role in the world simulator, as discussed in section 3.2.1. This is particularly important because humans are the most essential participants in the real world, making their realistic simulation crucial. Thanks to the early success in generative models, there are some representative works [37], [89], [90] that introduce generative adversarial networks (GAN) [14] for animating humans in videos. Despite these progresses, the most essential problem in human video animation is the visual fidelity of the generated videos. ControlNet [91] and HumanSD [92] are plug-and-play methods for animating humans referring to poses based on a foundation text-to-image model, like Stable Diffusion [31]. Additionally, to resolve the generalization issue of these methods, animate-anyone [93] proposes a ReferenceNet to maintain more spatial details of the reference video and pushes generation quality in the wild to a new milestone. There are some follow-up works [94], [95] of animate-anyone trying to simplify the training architecture and costs. Besides, as the in-depth study of geometry and textures in the computer graphics area, there are some works that introduce 3D modeling into human video animation. Liquid Warping GAN [96], CustomHuman [97] and LatentMan [98] are early attempts introducing 3D human prior into the generation loop. The latest progress, MIMO [99], explicitly models the character, 3D motion, and scene respectively to drive human animation in the wild. These methods with or without 3D priors make a great step to introduce humans into the loop of the world simulator.

## 3.3 3D Generation

3D generation focuses on both geometry and appearance to better simulate real-world scenarios. In this section, we explore various 3D representations and generation algorithms, providing a structured overview of recent advancements. Specifically, we categorize 3D generation methods based on their input modalities, including *Text-to-3D Generation*, which directly synthesizes 3D content from textual descriptions, *Image-to-3D Generation*, which introduces image constraints to refine text-driven outputs, and *Video-to-3D Generation*, which leverages video priors for more consistent 3D generation. A chronological summary of these advance-

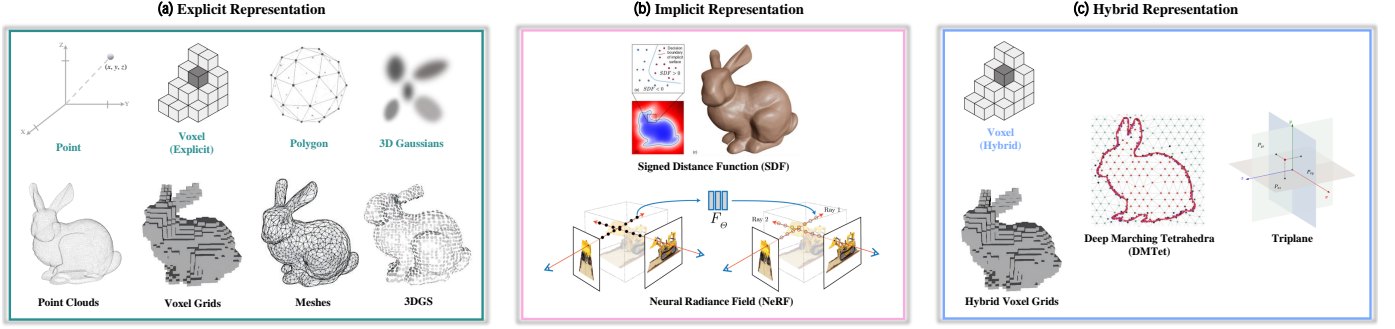


Fig. 3: Three main categories of neural scene representations. (a) Explicit representation stores geometry directly using point clouds, voxel grids [100], meshes [101], and 3D Gaussians [102]. (b) Implicit representation defines objects through functions like Signed Distance Functions (SDF) [103] and Neural Radiance Fields (NeRF) [104], enabling smooth, continuous surfaces without fixed resolution. (c) Hybrid representation combines explicit and implicit methods, using techniques like Hybrid Voxel Grids, Deep Marching Tetrahedra (DMTet) [105], and Triplanes for better efficiency and flexibility.

ments is presented in Figure 4, while Table 2 offers a comprehensive comparison of cutting-edge methods. Notably, several approaches span multiple categories, demonstrating the versatility of modern 3D generation techniques.

### 3.3.1 3D Representation

In the domain of 3D generation, the choice of an optimal 3D representation is crucial. For neural scene representation, 3D data can be typically divided into three main categories: explicit, implicit, and hybrid representations, which are illustrated in Figure 3.

**(1) Explicit Representations.** Explicit representations offer precise visualizations of objects and scenes, defined by a set of elements. Traditional forms, such as point clouds, meshes, and voxels, have been widely used for years.

**(i) Point Clouds** are unordered sets of 3D points  $(x, y, z)$  and often enriched with attributes like color or normals. While widely used due to depth sensor output, their irregular structure [106], [107] challenges conventional neural networks in 2D domains.

**(ii) Voxel Grids** are composed of basic elements called voxels. A voxel, as a 3D counterpart of a pixel [108], represents points on a 3D grid. It subdivides a bounding box into smaller elements, each with an occupancy value. While voxels can store data like opacity or color, they are memory-inefficient for high-resolution data due to cubic memory growth ( $\mathcal{O}(n^3)$ ) and sparse occupancy.

**(iii) Meshes** composed of vertices and edges forming polygons (faces), define two-dimensional surfaces in three-dimensional space. They are more memory-efficient than voxel grids by encoding only object surfaces and, unlike point clouds, provide explicit connectivity, enabling geometric transformations and efficient texture encoding.

**(iv) 3D Gaussian Splatting (3DGS)** is proposed as an effective method for accelerating both training and rendering tasks [102]. This technique models objects as collections of anisotropic Gaussian distributions, where each distribution is defined by its position (i.e., mean  $\mathbf{x} \in \mathbb{R}^3$ ), covariance matrix  $\Sigma$ , opacity  $\alpha \in \mathbb{R}$ , and spherical harmonics coefficients  $\mathbf{C} \in \mathbb{R}^k$  (with  $k$  representing the degrees of freedom), allowing for the modeling of view-dependent color variations, which is expressed as:

$$G(\mathbf{x}) = e^{-\frac{1}{2}\mathbf{x}^T \Sigma^{-1} \mathbf{x}}. \quad (6)$$

To facilitate optimization, the covariance matrix  $\Sigma$  is typically factorized into a scaling matrix  $\mathbf{S}$  and a rotation matrix  $\mathbf{R}$ , such that:

$$\Sigma = \mathbf{R} \mathbf{S} \mathbf{S}^T \mathbf{R}^T. \quad (7)$$

**(2) Implicit Representations.** Implicit representations describe 3D spaces with continuous functions, such as mathematical models or neural networks, capturing volumetric properties rather than surface geometry. Implicit neural representations approximate these functions with neural networks, enhancing expressiveness at the cost of higher training and inference overhead. Key approaches include Signed Distance Field (SDF) [103] and Neural Radiance Field (NeRF) [109].

**(i) Signed Distance Field (SDF)** is used to represent 3D shapes via neural fields, where a surface is implicitly defined as the zero-level set of the SDF. Given a point  $\mathbf{x} \in \mathbb{R}^3$ , the SDF function  $f(\mathbf{x}) = d$  returns the shortest distance to the nearest surface point, with the sign indicating whether  $\mathbf{x}$  lies inside ( $d < 0$ ) or outside ( $d > 0$ ) the shape. The surface is defined by the set of points where  $f(\mathbf{x}) = 0$ . The accuracy of SDFs relies on precise normal vectors, as their orientation determines distance signs, making accurate normal estimation essential for surface representation.

**(ii) Neural Radiance Field (NeRF)** [104], [109] represents 3D scenes as continuous volumetric functions encoded in the weights of a Multi-Layer Perceptron (MLP). Unlike DeepSDF [103], NeRF regresses density and color instead of a signed distance function, allowing for volumetric rendering. Specifically, NeRF maps spatial positions  $\mathbf{x} \in \mathbb{R}^3$  and viewing directions  $\mathbf{d} \in \mathbb{R}^2$  to density  $\sigma$  and color  $c$ , i.e.,  $f(\mathbf{x}, \mathbf{d}) = (\sigma, c)$ , using an MLP trained on images with known camera poses. To render a pixel, NeRF casts a ray  $\mathbf{r}(t) = \mathbf{o} + t\mathbf{d}$  from the camera into the scene and samples points along the ray at intervals  $t_i$ . The final pixel color  $C(\mathbf{r})$  is computed via volume rendering as:

$$C(\mathbf{r}) = \sum_i T_i \alpha_i c_i, \quad \text{where } T_i = \exp\left(-\sum_{k=0}^{i-1} \sigma_k \delta_k\right), \quad (8)$$

the term  $\alpha_i = 1 - \exp(-\sigma_i \delta_i)$  here represents the opacity of the sampled point, and the accumulated transmittance  $T_i$  quantifies the probability that the ray travels from  $t_0$  to  $t_i$  without being occluded by any particles. The term  $\delta_i =$



$t_i - t_{i-1}$  denotes the distance between consecutive sampled points along the ray.

**(3) Hybrid Representations.** Most current implicit methods depend on regressing NeRF or SDF values, which can limit their capacity to leverage explicit supervision on target views or surfaces. Explicit representations, however, offer useful constraints during training and improve user interaction. To leverage the complementary strengths of both paradigms, hybrid representations can be seen as a trade-off between explicit and implicit representations.

**(i) Hybrid Voxel Grids** can be used as hybrid representations in methods like [110]–[112]. [111] employs density and feature grids for radiance field reconstruction, while Instant-NGP [112] uses hash-based multi-level grids, optimizing GPU performance for faster training and rendering.

**(ii) DMTet** [105] combines tetrahedral grids with implicit SDF for flexible 3D surface representation. A neural network predicts SDF values and position offsets for each vertex, allowing the modeling of complex topologies. The grids are converted into meshes via a differentiable Marching Tetrahedra (MT) layer, enabling efficient, high-resolution rendering. By optimizing geometry and topology with mesh-based losses, DMTet achieves finer details, fewer artifacts, and outperforms previous methods in conditional shape synthesis from coarse voxels on complex 3D datasets.

**(iii) Tri-plane** provides a memory-efficient alternative to voxel grids for 3D shape representation and neural rendering. It decomposes 3D volumes into three orthogonal 2D feature planes ( $XY, XZ, YZ$ ). EG3D [113] utilizes this structure, employing an MLP to aggregate features from the planes and predict color and density values at any 3D point:  $(\sigma, c) = \text{MLP}(\mathbf{f}_{xy}(\mathbf{x}) + \mathbf{f}_{xz}(\mathbf{x}) + \mathbf{f}_{yz}(\mathbf{x}))$ . This approach reduces memory consumption compared to voxel-based NeRF and enables faster rendering.

### 3.3.2 Algorithms

**(1) Text-to-3D Generation.** To generate 3D content from the text prompt by simulating the geometrics in the real world, extensive studies have been conducted and can be divided into three branch. Readers can refer to [161]–[163] for a more comprehensive survey in this field.

**(i) Feedforward Approaches.** Motivated by text-to-image generation, a primary branch of methods extend existing successful generative models to directly synthesize 3D representations from the text prompt in one feedforward propagation. The key to success lies in encoding the 3D geometry into a compact representation and align it with the corresponding text prompt.

Michelangelo [122] first constructs a VAE model to encode 3D shapes into a latent embedding. Then, this embedding is aligned with the ones extracted from language and image using a CLIP [23] model. Using a contrastive loss for optimization, a 3D shape can be inferred from the text prompt. ATT3D [116] uses Instant-NGP model as the 3D representation and bridges it with the text embedding using a mapping network. Then, multi-view images are rendered from the Instant-NGP model and the whole network is optimized using SDS loss. Motivated by ATT3D, Atom [123] learns to predict a triplane representation from the text embedding and employs a two-stage optimization strategy.

Hyperfields [121] trains a dynamic hypernet to record the NeRF parameters learned from diverse scenes.

Recently, the impressive performance of diffusion models has motivated researchers to extend them to 3D generation. Early methods focus on learning to synthesize explicit 3D representations from the text prompt. Specifically, Point-E [114] first employs GLIDE [164] to synthesize multiple views, which are then used as conditions to produce a point cloud using a diffusion model. Later, MeshDiffusion [119] employ diffusions to build a mapping from text to meshes. Subsequent methods make attempts to applying diffusion models on implicit 3D representations. Shap-E [120] first maps 3D contents to parameters of a radiance field and then trains a diffusion model to generate these parameters conditioned on the text embedding. 3D-LDM [115] employs an SDF to represent the geometry of the 3D content and trains a diffusion model for text-conditioned generation. Similarly, Diffusion-SDF [117] constructs an SDF autoencoder with a voxelized diffusion model to generate voxelized signed distance fields (SDFs) from the text prompt. LATTE3D [118] develops a texture network and a geometry network to generate NeRF and SDF conditioned on the text embedding, respectively. Then, a 3D-aware diffusion model is optimized through an SDS loss.

**Discussion.** Compared with optimization-based approaches, feedforward approaches favor high efficiency and is capable of generating 3D contents without test-time optimization. These approaches, however, rely heavily on the quantity of data and usually suffer inferior structure and texture details.

**(ii) Optimization-based Approaches.** On top of text-to-image generation, another branch of methods optimize 3D representations by leveraging powerful text-to-image generative models to provide rich supervision.

DreamFusion [127] first introduces score distillation sampling (SDS) loss to optimize NeRFs using images synthesized from text prompts. MVDream [131] fine-tunes a multi-view diffusion model to generate multi-view images with cross-view consistency to train a NeRF to capture 3D contents. Magic3D [124] employs textured meshes to represent the 3D object and adopts SDS loss for optimization of the meshes. Dream3D [125] first generates an image from the text prompt, which is then employed to produce the 3D shape to initialize a neural radiance field. Next, a NeRF is optimized using the CLIP guidance. Fantasia3D [126] further combines DMTet and SDS loss to generate a 3D object from the text prompt. ProlificDreamer [128] develops variational score distillation (VSD) to model the distribution of 3D representations and produces higher-quality results with rich details. To address the multi-face Janus issue, PI3D [129] first fine-tunes the text-to-image diffusion model to produce pseudo-images. Then, these images are adopted to generate a 3D shape using an SDS loss. VP3D [130] first uses a text-to-image diffusion model to generate a high-quality image from the text prompt. Then, 3D representations are optimized via SDS loss using the resultant image and the text prompt as conditions.

With remarkable advances in 3D Gaussian, it is widely studied in the field of text-to-3D generation. DreamGaussian [132] first employs a diffusion to obtain 3D Gaussians with SDS loss being used for optimization. Then, meshes are





TABLE 2: Recent text-to-3D, image-to-3D and video-to-3D generation methods.

Paradigms	Methods	Paper	Code	Representations	Objectives
Text-to-3D	Feedforward	Point-E [114]	<a href="#">Link</a>	Point Clouds	MAE
		3D-LDM [115]	<a href="#">Link</a>	SDF	reconstruction+regularization
		ATT3D [116]	<a href="#">Link</a>	Instant-NGP model	SDS
		Diffusion-SDF [117]	<a href="#">Link</a>	SDF	reconstruction+KL-Divergence
		LATTE3D [118]	<a href="#">Link</a>	NeRF/SDF	SDS+regularization
		MeshDiffusion [119]	<a href="#">Link</a>	Mesh	diffusion loss
		Shap-E [120]	<a href="#">Link</a>	NeRF	rendering loss
		Hyperfields [121]	<a href="#">Link</a>	NeRF	SDS
		Michelangelo [122]	<a href="#">Link</a>	Occupancy Field	text-image-shape contrastive + BCE
		Atom [123]	<a href="#">Link</a>	Triplane	SDS
	Optimization	Magic3D [124]	<a href="#">Link</a>	NeRF/DMTet	SDS
		Dream3D [125]	<a href="#">Link</a>	NeRF	reconstruction+regularization
		Fantasia3D [126]	<a href="#">Link</a>	DMTet	SDS
		DreamFusion [127]	<a href="#">Link</a>	NeRF	SDS
		ProlificDreamer [128]	<a href="#">Link</a>	NeRF	VSD
		PI3D [129]	<a href="#">Link</a>	Triplane	SDS
		VP3D [130]	<a href="#">Link</a>	NeRF	SDS
		MVDream [131]	<a href="#">Link</a>	NeRF	SDS
		DreamGaussian [132]	<a href="#">Link</a>	3DGS	SDS
		GaussianDreamer [133]	<a href="#">Link</a>	3DGS	SDS
Image-to-3D	Feedforward	GSGEN [134]	<a href="#">Link</a>	3DGS	SDS
		Sculpt3D [135]	<a href="#">Link</a>	NeRF	diffusion loss
		Instant3D [136]	<a href="#">Link</a>	Triplane	MSE+LPIPS
		Direct2.5 [137]	<a href="#">Link</a>	Multi-view normal maps	normal rendering+alpha mask loss
		Sherpa3D [138]	<a href="#">Link</a>	DMTet	SDS
	Optimization	3DGen [139]	<a href="#">Link</a>	DMTet	rendering loss
		Shap-E [120]	<a href="#">Link</a>	NeRF	rendering loss
		Michelangelo [122]	<a href="#">Link</a>	Occupancy Field	text-image-shape contrastive + BCE
		Clay [140]	<a href="#">Link</a>	Occupancy Field	BCE
		CraftsMan [141]	<a href="#">Link</a>	Occupancy Field	BCE
		Direct3D [142]	<a href="#">Link</a>	Occupancy Field	BCE
		Trellis [143]	<a href="#">Link</a>	3DGS/RF/Mesh	MSE
		RealFusion [144]	<a href="#">Link</a>	NeRF	SDS/Image Reconstruction
		Zero123 [145]	<a href="#">Link</a>	NeRF	SDS
		Magic123 [146]	<a href="#">Link</a>	NeRF	SDS
Video-to-3D	MVS	SyncDreamer [147]	<a href="#">Link</a>	NeRF	SDS
		Consistent123 [148]	<a href="#">Link</a>	NeRF	SDS
		Toss [149]	<a href="#">Link</a>	NeRF	SDS
		ImageDream [150]	<a href="#">Link</a>	NeRF	SDS
		Wonder3D [151]	<a href="#">Link</a>	Mesh	Image/Normal MSE
		One-2-3-45 [152]	<a href="#">Link</a>	SDF	Image/Depth MSE
		CRM [153]	<a href="#">Link</a>	Triplane	Image/Depth MSE
		InstantMesh [154]	<a href="#">Link</a>	Triplane	Image/Depth/Normal MSE
		LRM [155]	<a href="#">Link</a>	NeRF	MSE
		Unique3D [156]	<a href="#">Link</a>	Mesh	Image/Normal MSE
Video-to-3D	MVS	ViVid-1-to-3 [87]	<a href="#">Link</a>	Multi-view images	-
		IM-3D [157]	<a href="#">Link</a>	3DGS	MSE+LPIPS
		V3D [158]	<a href="#">Link</a>	Mesh	MSE+LPIPS
		SV3D [159]	<a href="#">Link</a>	NeRF / DMTet	MSE+LPIPS
		CAT3D [160]	<a href="#">Link</a>	NeRF	MSE+LPIPS

the image models and the Multi-view consistency from 3D datasets, which significantly mitigates the Janus problem.

A series of works have expanded upon Zero123 [145]. Zero123-xl [168] pretrains Zero123 pipelines on a  $10\times$  larger 3D datasets for better generalization. Magic123 [146] leverages 2D and 3D priors simultaneously for distillation to manage the trade-off between generalization and consistency, and uses coarse-fine pipeline for higher quality. SyncDreamer [147] and Consistent123 [148] both further improves the multi-view consistency of NVS models by introducing a synchronized multi-view diffusion model, when the former leverages 3D volume to model joint distribution relations of images and the latter utilizes cross-view attention and shared self-attention. Toss [149] additionally brings text caption as high-level semantics of 3D data into the NVS model pretraining for stronger plausibility and controllability of invisible views. ImageDream [150] addresses both multi-view consistency and 3D details problem by designing a multi-level image-prompt controller and training with text descriptions. Wonder3D [151] incorporates the cross-domain attention mechanism, enabling the NVS model to simultaneously denoise images and align normal

maps, when introducing normal maps into the optimization process additionally.

**Discussion.** Inheriting the powerful priors of image generation models, optimization-based methods demonstrate strong generalization capabilities and can model high-precision textures. However, since novel view synthesis (NVS) models only use 2D data sampled from 3D rather than directly 3D data for supervision during pretraining, the multi-view consistency problem cannot be fundamentally resolved, despite improvements through 3D volume modeling or cross-view attention. Consequently, optimization-based methods often suffer from overly smooth geometries and long times for training due to the optimization paradigm.

**(iii) MVS-based Approaches.** MVS-based methods split the image-3D generation into two stages: first generate multi-view images from a single image using an NVS model, then directly create 3D assets from these multi-view images using a feedforward reconstruction network.

Based on the multi-view images predicted by Zero123 [145], One-2-3-45 [152] proposes an elevation estimation module and utilizes an SDF-based generalizable neural sur-

face reconstruction module pretrained on 3D datasets for 360° mesh reconstruction, which reduces the reconstruction time to 45 seconds compared to optimization-based. CRM [153] further freeze the output images of the multi-view generation model to six fixed camera poses, largely improving the consistency between multi-views. Then CRM input multi-view images into a convolutional U-Net to create a high-resolution triplane supervised by depth and RGB images. InstantMesh [154] also freeze the camera poses of multi-view images, but employ a transformer-based multi-view reconstruction model based on LRM [155] to reconstruct 3D meshes, providing better generalization at the expense of some image-3D detail consistency. Unique3d [156] introduce a multi-level upscale strategy to progressively generate higher-resolution multi-view images, and a normal map diffusion model to predict multi-view normal maps for the initialization of coarse meshes, which is refined and colored based on multi-view images.

**Discussion.** Compared with optimization-based methods, MVS-based methods train a feedforward reconstruction model on 3D datasets to reconstruction a high-quality 3D from multi-view images, significantly improving the 3D consistency and reducing inference time to seconds level. However, MVS-based methods often lack high-quality geometry details due to the limitation of the model scale.

**(3) Video-to-3D Generation.** The vast corpus of online video data serves as a rich repository of 3D information, capturing object motions, viewpoint variations, and camera transitions that unveil multi-view perspectives often unavailable in static imagery [172]–[177]. This dynamic content provides both temporal coherence and spatial consistency across sequential frames, which are essential for understanding complex 3D scenes and generating high-fidelity 3D structures [13]. As a result, leveraging these multi-view and time-variant data has become a promising approach for reconstructing and synthesizing 3D-consistent objects [178]. Recent research explores video-based priors for robust 3D generation [158]–[160], aiming to learn 3D representations that maintain coherence across frames and adapt to changing viewpoints. At high-level, the main idea of these works for video-to-3D generation is to enable a camera-controllable video model as a consistent multi-view generator for dense 3D reconstruction.

Recent advancements in video diffusion models have illuminated their exceptional capabilities in generating realistic videos while providing implicit reasoning about 3D structures. However, significant challenges persist in employing these models for effective 3D generation, particularly regarding precise camera control. Traditional models [179]–[181] are typically confined to generating clips with smooth and short camera trajectories, limiting their ability to create dynamic 3D scenes or integrate varying camera angles effectively. To address these limitations, several innovative techniques have been developed to enhance camera control within video diffusion frameworks. One early approach is AnimateDiff [49], which employs Low-Rank Adaptation (LoRA) [182] to fine-tune video diffusion models with fixed camera motion types. This method facilitates the synthesis of structured scenes while adhering to specified camera dynamics. Another significant advancement is MotionCtrl [183], which introduces conditioning

mechanisms that allow models to follow arbitrary camera paths, thereby enabling greater flexibility in generating diverse perspectives and overcoming the rigidity of previous methods. Based on the availability of camera-controllable video generation, SVD-MV [184], SV3D [159], and IM-3D [157] explore how to leverage camera control to improve the generation of 3D objects from video data. For example, SV3D trains a video diffusion model capable of rendering arbitrary views, which demonstrates enhanced generalization and high-resolution output (576×576 pixels). Such capability allows for maintaining spatial coherence across frames while adapting to various viewpoints, effectively addressing critical challenges in dense reconstruction. While effective, these methods often restrict camera movements to fixed, orbital paths surrounding central objects, which limits their applicability to complex scenes with rich contextual backgrounds. However, many of these methods still fall short when producing compelling 3D representations of intricate environments, where varying camera angles and interactions with multiple objects are crucial.

As controlling camera movements in video models complement novel view information, several methods have explored the potential of video diffusion models for novel view synthesis (NVS). For example, Vivid-1-to-3 [87] effectively merges a view-conditioned diffusion model with a video diffusion model, allowing for the generation of temporally consistent views. By ensuring smooth transitions across frames, this model enhances the quality of the synthesized output, making it particularly effective for 3D scene representations. CAT3D [160] augments rich multi-view information with a multi-view diffusion model.

**Discussion.** Leveraging video priors in multi-view generation transforms video diffusion models into consistent multi-view generators for dense 3D reconstruction. Further exploration will enhance high-fidelity 3D representation, especially for complex, dynamic environments requiring robust multi-view synthesis.

### 3.3.3 Applications

**(1) Avatar Generation.** With the emergence of the metaverse and the popularity of VR/AR, 3D avatar generation has drawn increasing interests. Early works focus on generating head avatars [185]–[187], which leverage text-to-image diffusion models and neural radiance fields to create facial assets. Later methods pay more attention to realistic full-body avatars generation by integrating neural radiance fields with statistical models [188], [189]. Recently, the animation capability of avatar generation has gained great attention with numerous methods being proposed [190], [191].

**(2) Scene Generation.** In addition to avatar generation, scene generation to create a realistic 3D environment is also highly demanded in applications like metaverse and embodied intelligence. Early methods focus on object-centered scenes and leverage conditional diffusion models to synthesize multi-view images to optimize neural radiance fields [115], [117]. Later works extend these methods to room-scale scenes by introducing progressive strategies [192], [193]. Motivated by their success, recent studies further investigate the generation of outdoor scenes, ranging from street-scale [194], [195] to city-scale [196], [197].

**(3) 3D Editing.** The powerful 3D generation capability has created the downstream application of 3D content editing. Several methods focus on changing the appearance or geometry of the 3D content globally [198], [199] without isolating a specific region from a scene. For example, scene stylization methods [200], [201] aims to manipulate the style of a 3D asset, such as illumination tuning and climate changes. Recent efforts are made to achieve flexible 3D content editing at a finer-grained level. Specifically, appearance change [202], [203], geometry deformation [204], [205], and object-level manipulation [206], [207] have been studied, with promising editing results being achieved.

### 3.4 4D Generation

We culminate in 4D generation by integrating all dimensions. As a cutting-edge field in computer vision, 4D generation focuses on synthesizing dynamic 3D scenes that evolve temporally based on multimodal inputs such as text, images, or videos. Unlike traditional 2D or 3D generation [208], 4D synthesis introduces unique challenges, requiring both spatial coherence and temporal consistency while balancing high fidelity, computational efficiency, and dynamic realism [209]. In this section, we first introduce 4D representation, which builds upon 3D representation, and then summarize current 4D generation methods. Recent research has explored two primary paradigms: optimization-based methods leveraging Score Distillation Sampling (SDS) and feedforward-based approaches that avoid per-prompt optimization. These paradigms address distinct technical challenges, highlighting the field’s complexity and the ongoing pursuit of a feasible balance among visual quality, computational efficiency, and scene flexibility. Representative works in 4D generation are summarized in Table 3.

#### 3.4.1 4D Representation

The field of 4D representation, which incorporates a temporal dimension into 3D modeling, provides a strong foundation for understanding dynamic scenes. By extending static 3D spatial representations  $(x, y, z)$  with time  $(t)$ , these methods encode scene dynamics and transformations, essential for applications such as non-rigid human motion capture and simulating object trajectories [230]–[233].

A major challenge in 4D representation is the high computational cost of reconstructing a single scene. To address this, explicit and hybrid methods enhance efficiency without sacrificing quality. For instance, planar decompositions streamline 4D spacetime grids by breaking them into smaller components [234]–[236], while hash-based representations reduce memory and processing requirements [237]. 3DGS balances speed and quality by using deformation networks to adapt static Gaussians to dynamic ones [102], [238].

Recent advances disentangle static and dynamic scene components to render both rigid and non-rigid motions efficiently. For example, D-NeRF first encodes scenes into a canonical space and then maps them into temporally deformed states [239]. 3D Cinemagraphy generates feature-based point clouds from single images and animates using 3D scene flow [240]. 4DGS captures temporal dynamics by modeling attributes like scales, positions, and rotations as time functions while keeping static scene unchanged [241].

Hybrid NeRF-based methods expand 4D modeling with plane- and voxel-based feature grids. These grids, combined with MLPs, enable efficient novel-view synthesis and extend to dynamic scenes by incorporating temporal planes [234], [235]. Deformable NeRFs separate geometry and motion, simplifying motion learning and supporting applications like image-to-4D video generation and multi-view reconstruction [112]. Collectively, these advancements reflect ongoing progress in achieving computationally efficient, high-quality temporal modeling for dynamic scenes.

#### 3.4.2 Algorithms

**(1) Feedforward Approaches.** Feedforward-based methods provide an efficient alternative by generating 4D content in a single forward pass, bypassing the iterative optimization required in SDS-based pipelines. These methods rely on pre-trained models, leveraging temporal and spatial priors to achieve fast and consistent generation. Control4D [210] and Animate3D [211] directly synthesize dynamic scenes from textual or visual inputs, enabling real-time applications such as interactive media and personalized content creation. Vidu4D [212] improves motion trajectories by incorporating temporal priors, ensuring frame-to-frame coherence and smooth transitions. Diffusion4D [213] extends the capabilities of diffusion models to handle 4D scene synthesis by combining spatial-temporal feature extraction with efficient inference mechanisms. L4GM [214] further enhances feedforward techniques by integrating latent geometry modeling, producing high-quality results while maintaining computational efficiency.

**Discussion.** Feedforward-based approaches excel in scenarios that prioritize speed and adaptability, such as real-time content generation and lightweight deployment on consumer devices. However, their reliance on pre-trained models and limited flexibility in handling complex dynamics pose challenges in achieving the same level of detail and diversity as optimization-based methods. Despite these limitations, feedforward techniques represent a significant step toward practical 4D generation, addressing key challenges of computational efficiency and scalability. By bridging the gap between quality and speed, these methods are poised to play a critical role in advancing 4D content generation for a wide range of applications.

**(2) Optimization-based Approaches.** Optimization-based methods are foundational in 4D generation, employing iterative techniques such as Score Distillation Sampling (SDS) to adapt pre-trained diffusion models to synthesize dynamic 4D scenes. These approaches leverage powerful priors from text-to-image, multi-view image, and text-to-video generation models, achieving temporally coherent scenes with rich motion dynamics. For example, MAV3D [215] optimizes NeRF or HexPlane features against SDS loss guided by textual prompts, while 4D-fy [216] and Dream-in-4D [219] improve the 3D consistency and motion dynamics by integrating image, multi-view, and video diffusion models in SDS supervision. AYG [217] proposes to use deformable 3DGS as inherent representation, which can easily disentangle static geometry from dynamic motion with a simple delta deformation field to improve flexibility.



TABLE 3: Representative works of 4D generation methods. "Rep" stands for representations.

Approaches	Methods	Paper	Code	Representations	Priors / Models	Objectives
Feedforward	Control4D [210]	<a href="#">Link</a>	-	GaussianPlanes	GAN-based	GAN objective
	Animate3D [211]	<a href="#">Link</a>	<a href="#">Link</a>	4DGS	Diffusion-based	latent diffusion loss
	Vidu4D [212]	<a href="#">Link</a>	<a href="#">Link</a>	Dynamic Gaussian Surfels	Diffusion-based	reconstruction/regularization loss
	Diffusion4D [213]	<a href="#">Link</a>	<a href="#">Link</a>	4DGS	Diffusion-based	latent diffusion + motion reconstruction loss
	L4GM [214]	<a href="#">Link</a>	<a href="#">Link</a>	3DGS	VAE-based	MSE+LPIPS
Optimization	MAV3D [215]	<a href="#">Link</a>	-	HexPlane-7/NeRF-based 4D Rep	T2I/T2V	SDS
	4D-fy [216]	<a href="#">Link</a>	<a href="#">Link</a>	Hash-/NeRF-based 4D Rep	MVDream/T2I/T2V	Hybrid SDS
	AYG [217]	<a href="#">Link</a>	-	Deformable 3DGS	MVDream, T2I/T2V	SDS variant(CSD [218])
	Dream-in-4D [219]	<a href="#">Link</a>	<a href="#">Link</a>	NeRF-based 4D Rep	MVDream/T2I/T2V	Hybrid SDS
	TC4D [220]	<a href="#">Link</a>	<a href="#">Link</a>	Hash-/NeRF-based 4D Rep	T2V	SDS
	4Real [221]	<a href="#">Link</a>	-	Deformable 3DGS	T2V	SDS
	C3V [222]	<a href="#">Link</a>	-	3DGS	LDMs [31]	SDS
	Consistent4D [223]	<a href="#">Link</a>	<a href="#">Link</a>	D-NeRF	Zero123	SDS
	SC4D [224]	<a href="#">Link</a>	<a href="#">Link</a>	SC-GS [225]	SVD/Zero123	SDS
	STAG4D [226]	<a href="#">Link</a>	<a href="#">Link</a>	Deformable 3DGS	SVD/Zero123	SDS
	DreamScene4D [227]	<a href="#">Link</a>	<a href="#">Link</a>	Deformable 3DGS	SVD/Zero123	SDS
	4DM [228]	<a href="#">Link</a>	<a href="#">Link</a>	D-NeRF	SVD	4D-aware SDS + anchor loss
	DreamMesh4D [229]	<a href="#">Link</a>	<a href="#">Link</a>	SC-GS+Mesh Rep	Zero123	SDS

Based on such pipelines, recent works further improve 4D generation from multiple aspects: appearance quality, geometry consistency, motion faithfulness, and generation controllability. In particular, TC4D [220] and SC4D [224] enable free user control on 4D object motion trajectory. STAG4D [226] employs multi-view fusion to enhance spatial and temporal alignment across frames, ensuring smooth transitions and consistency. Additionally, DreamScene4D [227] and DreamMesh4D [229] adopt disentanglement strategies to localize optimization efforts, significantly reducing computational overhead while maintaining high fidelity. Recent advances such as 4Real [221] and C3V [222] further push the boundaries of optimization-based methods by combining compositional scene generation with efficient optimization. These methods break dynamic scenes into modular components such as static geometry and motion fields, enabling flexible updates and diverse content generation. Despite their strengths in achieving high-quality and temporally consistent results, optimization-based approaches remain computationally demanding, with runtime requirements often precluding real-time applications. As research progresses, ongoing efforts focus on improving scalability and reducing latency without compromising visual fidelity or dynamic realism.

### 3.4.3 Applications

**(1) 4D Editing.** Instruction-guided editing, which allows users to edit scenes through natural language, offers a user-friendly and intuitive approach. While this has been successfully achieved for 2D images with models like Instruct-Pix2Pix (IP2P) [281] and Instruct-NeRF2NeRF (IN2N) [199] for 3D scenes, extending this capability to 4D scenes presents significant challenges. Recent developments in text-to-image diffusion models and differentiable scene representations have enabled editing 4D scenes using text prompts. For instance, Instruct 4D-to-4D [282] treats 4D scenes as pseudo-3D scenes, adopting a video editing approach to iteratively generate coherent edited datasets. Concurrent work like Control4D [210] employs GANs alongside diffusion models to ensure consistent editing for dynamic 4D portraits based on text instructions.

**(2) Human Animation.** As an essential component of 4D simulation, human motion generation is a research branch that attracts the most attention from the community. Different from the human-centric video generation (in section 3.2.2), 3D human motion generation is easier to animate

characters in 3D applications, *e.g.* games and embodied intelligence. The recent success of the 3D human motion generation mainly comes from the well-studied human body parameterized models [283], [284].

The human motion generation aims to achieve a basic target: simulating 4D human subjects in the digital world, which can be divided into two folds. 1) *Generating motions with sparse control signals* mainly simulates human animations in the virtual world based on the sparse motions specified by users. Robust motion in-between [285] proposes a time-to-arrival embedding and the scheduled target noise vector to perform motion in-between with different transition lengths in a model robustly. As the phase manifold of the motion space has a good structure, Starke *et al.* [286] propose a mixture-of-expert network to in-between motions in the phase manifold. Besides, another part of sparse control-guided motion generation is motion prediction, *a.k.a* motion extrapolation. Early researches in motion prediction [287]–[290] try to predict motions in a deterministic way. Considering that motion prediction is subjective, several works [291]–[295] have proposed generating diverse motions in their predictions. 2) *Generating motions with multi-modality conditions* aims to simulate human motions with other modality inputs, *e.g.* text, audio, musics. To resolve the problem of limited pairwise text-motion data, Guo *et al.* [296] propose a relatively large text-motion dataset, HumanML3D, which is significantly larger than previous datasets and greatly pushes the development of the tasks. Besides, some researchers verify that VQ-VAE [296]–[301] is another effective fashion for synthesizing motions with text. With the rapid development of diffusion models, a lot of works [302]–[307] introduce diffusion models into the task and achieve good generation quality. Similar to the text-to-motion task [308]–[313], the technical roadmap of music-driven dance generation can also be divided into cVAE [314], VQ-VQE [315], and diffusion-based [316], [317] methods.

## 4 DATASETS AND EVALUATIONS

In this section, we summarize the commonly-used datasets for 2D, video, 3D, and 4D generation in Table 4. Then, we present a unified and comprehensive summary of evaluation metrics in Table 5. For quantitative analysis, we evaluate metrics from two perspectives: 1) *Quality*: assessing the perceptual quality of the synthesized data, independent of

TABLE 4: Summary of the widely-used 2D, video, 3D and 4D generation datasets. [Link] directs to dataset websites.

Dataset	Year	Numbers	Type	Evaluation Metrics	Contribution Highlights
<b>2D Generation (Sec. 3.1)</b>					
SBU [242] [Link]	2011	1M	Image-Text pairs	-	Photographs with captions and 5 kinds of image content.
MS-COCO [243] [Link]	2014	330K	Image-Text pairs	FID, CLIP-Score, SSIM	Manual annotation and 330K for English.
CC-3M [244] [Link]	2018	3M	Image-Text pairs	-	Alt-text caption annotation.
LAION-5B [169] [Link]	2022	5.85B	Image-Text pairs	FID, CLIP-Score, SSIM	5.85B CLIP-filtered multilingual image-text pairs.
ShareGPT4V [245] [Link]	2023	102K	Image-Text pairs	-	1.2M image-text pairs for ShareGPT4V-PT.
Pick-a-Pic [246] [Link]	2023	500K(35K distinct prompts)	Image-Text pairs	FID, PickScore	Human preferences on model-generated images.
<b>Video Generation (Sec. 3.2)</b>					
UCF-101 [247] [Link]	2012	13K	action recognition	FVD	Manual caption annotation.
ActivityNet [248] [Link]	2015	28K	action recognition	FVD	Manual caption annotation.
MSR-VTT [249] [Link]	2016	10K	video-language dataset	FVD, CLIP-Score	Manual caption annotation. Resolution: 240p.
HowTo100M [250] [Link]	2019	136M	video-language dataset	FVD, CLIP-Score	ASR annotation. Resolution: 240p.
WebVideo-10M [251]	2021	10M	video-language dataset	FVD, CLIP-Score	Alt-text caption annotation. Resolution: 360p.
HD-VILA-100M [252] [Link]	2022	103M	video-language dataset	FVD, CLIP-Score	ASR annotation. Resolution: 720p.
InternVid [253] [Link]	2023	7M	video-language dataset	FVD, CLIP-Score	Automatic caption annotation.
Panda-70M [170] [Link]	2024	70M	video-language dataset	FVD, CLIP-Score	Automatic caption annotation. Resolution: 720p.
Koala-36M [254] [Link]	2024	36M	video-language dataset	FVD, CLIP-Score	Automatic and manual caption annotation. Resolution: 720p.
<b>3D Generation (Sec. 3.3)</b>					
DeepFashion [255] [Link]	2016	800K	single-view images	-	Human clothing dataset.
SHHQ [256] [Link]	2022	40K	single-view images	-	Human body dataset.
C03D [257] [Link]	2021	19K(1.5M images)	multi-view images	PSNR/LPIPS; IoU, etc.	Image-to-3D Generation. 50 classes. Annotations: cameras, pcl.
RTMV [258] [Link]	2021	300K	multi-view images	PSNR/LPIPS; MAE, etc.	2,000 complex scenes with ray tracing (1600×1600).
MVImgNet [259] [Link]	2023	219K	multi-view images	PSNR/LPIPS	6.5M frames, 238 classes. Annotations: cameras, pcl.
uCO3D [260] [Link]	2025	170K	multi-view images	PSNR/LPIPS; IoU	1K classes. Annotations: cameras, 3DGS, captions.
ShapeNet [261] [Link]	2015	51K	3D data	-	51K 3D CAD models across 3K object categories.
3D-Future [262] [Link]	2020	10K	3D data	CLIP Similarity	9,992 3D furniture models with textures and attributes.
GSO [263] [Link]	2022	1K	3D data	F-Score/ CLIP Similarity	Image-to-3D Generation. 1,030 scanned household objects.
Objaverse [167] [Link]	2022	800K	3D data	F-Score/ CLIP Similarity	Objaverse and Objaverse-1.0 are the same.
Objaverse-XL [168] [Link]	2023	10.2M	3D data	F-Score/ CLIP Similarity	Image-to-3D Generation.
Cap3D [264] [Link]	2023	785k	3D-Text pairs	FID/CLIP etc.	Text-to-3D Generation. Auto/manual captions.
Animal2400 [116]	2023	Training(300), Testing(2400)	prompts	CLIP R-Precision	Text-to-3D Generation. 10 animals, 8 activities, 6 themes, 5 hats.
DreamFusion [127] [Link]	2024	DF27/DF415	prompts	CLIP R-Precision	Text-to-3D Generation. DF27: 27 paper prompts; DF415: 415 webpage prompts.
<b>4D Generation (Sec. 3.4)</b>					
Consistent4D [223] [Link]	2023	12(in-the-wild), 14(synthetic)	multi-view videos	LPIPS/CLIP	Video-to-4D Generation.
Diffusion4D [213] [Link]	2024	365K	dynamic 3D data	-	Collected from Objaverse-1.0 (42K) and Objaverse-xl (323K)
MV-Video [211] [Link]	2024	53K	dynamic 3D data	-	Annotated by MiniGPT4-Video [265]
CamVid-30K [266] [Link]	2024	30K	4D data	-	Real-world 4D scene dataset
4D-DRESS [267] [Link]	2024	64(outfits)	human clothing 4D data	CD	Total number of 3D human frames: 78k.

"ASR" stands for automatic speech recognition, "pcl" for point clouds, and "CD" for Chamfer Distance.

TABLE 5: Summary of common evaluation metrics.

Notation	Description
<b>Quality (quantitative analysis)</b>	
Image-level	PSNR ↑ <i>Image Fidelity/Similarity. Peak Signal-to-Noise Ratio: the ratio between the peak signal and the Mean Squared Error (MSE).</i>
	SSIM ↑ <i>Image Fidelity/Similarity. Structural Similarity Index Measure [268]: evaluating brightness, contrast, and structural features between generated and original images.</i>
	LPIPS ↓ <i>Image Fidelity/Similarity. Learned Perceptual Image Patch Similarity [269]: metric computed with a model trained on labeled human-judged perceptual similarity.</i>
	FID ↓ <i>Image Fidelity/Similarity. Fréchet Inception Distance [270]: comparison of generated and GT image distributions.</i>
	IS ↑ <i>Image Fidelity/Similarity. Inception Score [271]: metric only evaluated image distributions and calculated by pretrained Inception v3 model.</i>
Video-level	FVD ↓ <i>Video Fidelity. Fréchet Video Distance [272]: the Inflated-3D Convnets (I3D) pretrained model to compute their means and covariance matrices for scores.</i>
	KVD ↓ <i>Video Fidelity. Kernel Video Distance [272]: an alternative to FVD proposed in the same work, using a polynomial kernel.</i>
	Video IS ↑ <i>Video Fidelity. Video Inception Score [273]: the inception score of videos with the features extracted from C3D [274].</i>
	FVMD ↓ <i>Video Fidelity. Fréchet Video Motion Distance [275]: metric focused on temporal consistency, measuring the similarity between motion features of generated and reference videos using Fréchet Distance.</i>
<b>Alignment (quantitative analysis)</b>	
Semantics	CLIP Similarity [276] ↑ <i>Text-Image Alignment. Same as CLIP-Score, defined as a text-to-image similarity metric, measuring the (cosine) similarity of the embedded image and text prompt.</i>
	CLIP R-Precision [277] ↑ <i>Text-Image Alignment. The CLIP model's accuracy at classifying the correct text input of a rendered image from amongst a set of distractor query prompts.</i>
	X-CLIP [278] ↑ <i>Text-Image Alignment. Measured by a video-based CLIP model finetuned on text-video data.</i>
	CLIP-T ↑ <i>CLIP Textual Alignment. The average cosine similarity between the generated frames and text prompt with CLIP ViT-B/32 [279] image and text models.</i>
	CLIP-I ↑ <i>CLIP Image Alignment. The average cosine similarity between the generated frames and subject images with CLIP ViT-B/32 image model.</i>
	DINO-I ↑ <i>DINO [280] Image Alignment. The average visual similarity between generated frames and reference images with DINO ViT-S/16 model.</i>
<b>User study (qualitative analysis)</b>	
AQ ↑	<i>Human Preference. Appearance Quality: percentage unit (%).</i>
GQ ↑	<i>Human Preference. Geometry Quality: percentage unit (%).</i>
DQ ↑	<i>Human Preference. Dynamics Quality: percentage unit (%).</i>
TA ↑	<i>Human Preference. Text Alignment: percentage unit (%).</i>

input conditions (e.g., text prompts). 2) *Alignment*: measuring condition consistency, i.e., how well the generated data matches the user's intended input. For qualitative analysis, the visual quality of generated results plays a critical role in assessing methods. Therefore, we include some human preference-based indicators as references for more effectively conducting user studies, enabling more convincing qualitative analysis results.

## 5 FUTURE DIRECTIONS

Despite significant advancements in 2D, video, and 3D generation, 4D generation still faces substantial challenges. These difficulties are compounded by the complex nature

of integrating spatial and temporal dimensions. In 2D generation, key hurdles remain in improving realism and the diversity of generated images. For video generation, modeling long-term temporal dynamics and ensuring smooth transitions between frames are critical challenges. In 3D generation, balancing high-quality output with computational efficiency remains a key issue. Addressing these challenges is essential for advancing 4D generation, as it builds upon these established principles. Below, we outline the primary future directions for 4D generation, illustrating how solving these problems will not only benefit 4D models but also push forward progress in 2D, video, and 3D generation.

**Multi-Modal Generation:** Generating diverse and plausible

4D content that captures the inherent variability of real-world dynamics is a major challenge. Since real-world scenarios are usually multi-modal, current generative models often struggle to capture this diversity and tend to produce unrealistic results. Techniques like conditional generation or latent space modeling are being explored, but achieving both diversity and realism in multi-modal 4D generation remains an open problem.

**Temporal Consistency and Coherence:** Ensuring smooth and realistic transitions between frames over time is a significant challenge in 4D generation. Unlike static 3D generation, 4D generation requires maintaining consistency in shape, texture, and motion across time steps. Artifacts such as flickering or unnatural deformations can easily arise, especially in long sequences. Developing methods that enforce temporal coherence without sacrificing detail or realism remains an open problem.

**Physics and Dynamics Modeling:** Realistic 4D generation requires accurate modeling of physical interactions, such as collisions, deformations, and fluid dynamics. Incorporating physics-based constraints into generative models is challenging, as it often involves solving complex differential equations or simulating interactions in real time. Balancing realism with computational efficiency is an open problem.

**Generalization Across Scenarios:** 4D generation models often struggle to generalize across diverse scenarios, such as different object types, motion patterns, or environmental conditions. This is due to the high variability in dynamic 3D content and the limited diversity in training datasets. Developing models that can adapt to unseen scenarios without extensive retraining remains a challenge.

**Control and Editability:** Enabling flexible user control over 4D generation, such as specifying motion trajectories or editing dynamic content, is challenging. Current methods often lack fine-grained control, making it difficult to generate content that meets specific requirements. Developing intuitive interfaces and algorithms for interactive 4D editing is an open area of research.

**High Computational Cost:** 4D generation involves processing and storing vast amounts of data, as it requires modeling both spatial and temporal dimensions. This leads to high computational and memory requirements, making real-time or large-scale 4D generation difficult. Efficient compression techniques and scalable architectures are needed to address these challenges.

## 6 CONCLUSIONS

In this survey, we review recent progress and challenges in simulating the real world across appearance, dynamics, and geometry dimensions through the lens of multimodal generative models. We also summarize the commonly used datasets, their properties, and the corresponding evaluation metrics from various perspectives. Despite significant advancements, challenges in scalability, temporal coherence, and dynamic adaptability still remain. We provided open challenges to guide further researches towards more realistic real-world simulation.

## REFERENCES

- [1] Y. LeCun, "A path towards autonomous machine intelligence version 0.9. 2, 2022-06-27," *Open Review*, vol. 62, no. 1, pp. 1–62, 2022.
- [2] L.-H. Lee, T. Braud, P. Y. Zhou, L. Wang, D. Xu, Z. Lin, A. Kumar, C. Bermejo, P. Hui *et al.*, "All one needs to know about metaverse: A complete survey on technological singularity, virtual ecosystem, and research agenda," *Foundations and trends® in human-computer interaction*, vol. 18, no. 2–3, pp. 100–337, 2024.
- [3] J. Bruce, M. D. Dennis, A. Edwards, J. Parker-Holder, Y. Shi, E. Hughes, M. Lai, A. Mavalankar, R. Steigerwald, C. Apps *et al.*, "Genie: Generative interactive environments," in *ICML*, 2024.
- [4] P. Wu, A. Escontrela, D. Hafner, P. Abbeel, and K. Goldberg, "Daydreamer: World models for physical robot learning," in *CoRL*, 2023, pp. 2226–2240.
- [5] Y. Wang, J. He, L. Fan, H. Li, Y. Chen, and Z. Zhang, "Driving into the future: Multiview visual forecasting and planning with world model for autonomous driving," in *CVPR*, 2024, pp. 14749–14759.
- [6] D. Ha and J. Schmidhuber, "World models," *arXiv*, 2018.
- [7] J. W. Forrester, "Counterintuitive behavior of social systems," *Theory and decision*, vol. 2, no. 2, pp. 109–140, 1971.
- [8] Z. Zhu, X. Wang, W. Zhao, C. Min, N. Deng, M. Dou, Y. Wang, B. Shi, K. Wang, C. Zhang *et al.*, "Is sora a world simulator? a comprehensive survey on general world models and beyond," *arXiv*, 2024.
- [9] M.-M. Cheng, Q.-B. Hou, S.-H. Zhang, and P. L. Rosin, "Intelligent visual media processing: When graphics meets vision," *Journal of Computer Science and Technology*, vol. 32, pp. 110–121, 2017.
- [10] E. Catmull and A. R. Smith, "3-d transformations of images in scanline order," *ACM SIGGRAPH Computer Graphics*, vol. 14, no. 3, pp. 279–285, 1980.
- [11] N. Burtynk and M. Wein, "Computer-generated key-frame animation," *Journal of the SMPTE*, vol. 80, no. 3, pp. 149–153, 1971.
- [12] K. Erleben, "Physics based animation," *Charles River Media*, 2005.
- [13] T. Brooks, B. Peebles, C. Holmes, W. DePue, Y. Guo, L. Jing, D. Schnurr, J. Taylor, T. Luhman, E. Luhman, C. Ng, R. Wang, and A. Ramesh, "Video generation models as world simulators," 2024. [Online]. Available: <https://openai.com/research/video-generation-models-as-world-simulators>
- [14] I. Goodfellow, J. Pouget-Abadie, M. Mirza, B. Xu, D. Warde-Farley, S. Ozair, A. Courville, and Y. Bengio, "Generative adversarial networks," *Communications of the ACM*, vol. 63, no. 11, pp. 139–144, 2020.
- [15] D. P. Kingma, "Auto-encoding variational bayes," *arXiv preprint arXiv:1312.6114*, 2013.
- [16] Y. Bengio, R. Ducharme, and P. Vincent, "A neural probabilistic language model," in *NeurIPS*, vol. 13, 2000.
- [17] D. Rezende and S. Mohamed, "Variational inference with normalizing flows," in *ICML*, 2015, pp. 1530–1538.
- [18] J. Ho, A. Jain, and P. Abbeel, "Denosing diffusion probabilistic models," in *NeurIPS*, vol. 33, 2020, pp. 6840–6851.
- [19] A. Van den Oord, N. Kalchbrenner, L. Espeholt, O. Vinyals, A. Graves *et al.*, "Conditional image generation with pixelcnn decoders," in *NeurIPS*, 2016.
- [20] A. Jain, P. Abbeel, and D. Pathak, "Locally masked convolution for autoregressive models," in *UAI*, 2020.
- [21] E. Hoogeboom, A. A. Gritsenko, J. Bastings, B. Poole, R. van den Berg, and T. Salimans, "Autoregressive diffusion models," in *ICLR*, 2022.
- [22] C. Saharia, W. Chan, S. Saxena, L. Li, J. Whang, E. L. Denton, K. Ghasemipour, R. Gontijo Lopes, B. Karagol Ayan, T. Salimans *et al.*, "Photorealistic text-to-image diffusion models with deep language understanding," in *NeurIPS*, vol. 35, 2022, pp. 36479–36494.
- [23] A. Radford, J. W. Kim, C. Hallacy, A. Ramesh, G. Goh, S. Agarwal, G. Sastry, A. Askell, P. Mishkin, J. Clark *et al.*, "Learning transferable visual models from natural language supervision," in *ICML*, 2021, pp. 8748–8763.
- [24] J. Devlin, M.-W. Chang, K. Lee, and K. Toutanova, "Bert: Pre-training of deep bidirectional transformers for language understanding," *arXiv*, 2018.
- [25] C. Raffel, N. Shazeer, A. Roberts, K. Lee, S. Narang, M. Matena, Y. Zhou, W. Li, and P. J. Liu, "Exploring the limits of transfer learning with a unified text-to-text transformer," *Journal of Machine Learning Research*, vol. 21, no. 1, pp. 5485–5551, 2020.



- [26] A. Ramesh, M. Pavlov, G. Goh, S. Gray, C. Voss, A. Radford, M. Chen, and I. Sutskever, "Zero-shot text-to-image generation," in *ICML*, 2021, pp. 8821–8831.
- [27] A. Ramesh, P. Dhariwal, A. Nichol, C. Chu, and M. Chen, "Hierarchical text-conditional image generation with clip latents," *arXiv*, vol. 1, no. 2, p. 3, 2022.
- [28] OpenAI, "https://openai.com/index/dall-e-3/," 2024.
- [29] —, "https://openai.com/chatgpt/," 2024.
- [30] S. AI, "https://github.com/deep-floyd/if," 2024.
- [31] R. Rombach, A. Blattmann, D. Lorenz, P. Esser, and B. Ommer, "High-resolution image synthesis with latent diffusion models," in *CVPR*, 2022, pp. 10 684–10 695.
- [32] C. Schuhmann, R. Vencu, R. Beaumont, R. Kaczmarczyk, C. Mullis, A. Katta, T. Coombes, J. Jitsev, and A. Komatsuzaki, "Laion-400m: Open dataset of clip-filtered 400 million image-text pairs," *arXiv*, 2021.
- [33] D. Podell, Z. English, K. Lacey, A. Blattmann, T. Dockhorn, J. Müller, J. Penna, and R. Rombach, "Sdxl: Improving latent diffusion models for high-resolution image synthesis," *arXiv*, 2023.
- [34] B. F. Labs, "https://blackforestlabs.ai/," 2024.
- [35] M. Babaeizadeh, C. Finn, D. Erhan, R. H. Campbell, and S. Levine, "Stochastic variational video prediction," *arXiv*, 2017.
- [36] M. Babaeizadeh, M. T. Saffar, S. Nair, S. Levine, C. Finn, and D. Erhan, "Fitvid: Overfitting in pixel-level video prediction," *arXiv*, 2021.
- [37] S. Tulyakov, M.-Y. Liu, X. Yang, and J. Kautz, "Mocogan: Decomposing motion and content for video generation," in *CVPR*, 2018, pp. 1526–1535.
- [38] I. Skorokhodov, S. Tulyakov, and M. Elhoseiny, "Stylegan-v: A continuous video generator with the price, image quality and perks of stylegan2," in *CVPR*, 2022, pp. 3626–3636.
- [39] S. Yu, J. Tack, S. Mo, H. Kim, J.-W. Ha, and J. Shin, "Generating videos with dynamics-aware implicit generative adversarial networks," *arXiv*, 2022.
- [40] Y. Wang, L. Jiang, and C. C. Loy, "Styleinv: A temporal style modulated inversion network for unconditional video generation," in *ICCV*, 2023, pp. 22 851–22 861.
- [41] J. Ho, T. Salimans, A. Gritsenko, W. Chan, M. Norouzi, and D. J. Fleet, "Video diffusion models," in *NeurIPS*, vol. 35, 2022, pp. 8633–8646.
- [42] U. Singer, A. Polyak, T. Hayes, X. Yin, J. An, S. Zhang, Q. Hu, H. Yang, O. Ashual, O. Gafni *et al.*, "Make-a-video: Text-to-video generation without text-video data," *arXiv*, 2022.
- [43] J. Ho, W. Chan, C. Saharia, J. Whang, R. Gao, A. Gritsenko, D. P. Kingma, B. Poole, M. Norouzi, D. J. Fleet *et al.*, "Imagen video: High definition video generation with diffusion models," *arXiv*, 2022.
- [44] D. Zhou, W. Wang, H. Yan, W. Lv, Y. Zhu, and J. Feng, "Mag-icvideo: Efficient video generation with latent diffusion models," *arXiv*, 2022.
- [45] P. Esser, J. Chiu, P. Atighehchian, J. Granskog, and A. Germanidis, "Structure and content-guided video synthesis with diffusion models," in *ICCV*, 2023, pp. 7346–7356.
- [46] S. Ge, S. Nah, G. Liu, T. Poon, A. Tao, B. Catanzaro, D. Jacobs, J.-B. Huang, M.-Y. Liu, and Y. Balaji, "Preserve your own correlation: A noise prior for video diffusion models," in *ICCV*, 2023, pp. 22 930–22 941.
- [47] A. Blattmann, R. Rombach, H. Ling, T. Dockhorn, S. W. Kim, S. Fidler, and K. Kreis, "Align your latents: High-resolution video synthesis with latent diffusion models," in *CVPR*, 2023, pp. 22 563–22 575.
- [48] X. Wang, H. Yuan, S. Zhang, D. Chen, J. Wang, Y. Zhang, Y. Shen, D. Zhao, and J. Zhou, "Videocomposer: Compositional video synthesis with motion controllability," in *NeurIPS*, vol. 36, 2024.
- [49] Y. Guo, C. Yang, A. Rao, Z. Liang, Y. Wang, Y. Qiao, M. Agrawala, D. Lin, and B. Dai, "Animatediff: Animate your personalized text-to-image diffusion models without specific tuning," *arXiv*, 2023.
- [50] Y. Zeng, G. Wei, J. Zheng, J. Zou, Y. Wei, Y. Zhang, and H. Li, "Make pixels dance: High-dynamic video generation," in *CVPR*, 2024, pp. 8850–8860.
- [51] R. Girdhar, M. Singh, A. Brown, Q. Duval, S. Azadi, S. S. Rambhatla, A. Shah, X. Yin, D. Parikh, and I. Misra, "Emu video: Factorizing text-to-video generation by explicit image conditioning," *arXiv*, 2023.
- [52] O. Bar-Tal, H. Chefer, O. Tov, C. Herrmann, R. Paiss, S. Zada, A. Ephrat, J. Hur, G. Liu, A. Raj *et al.*, "Lumiere: A space-time diffusion model for video generation," in *SIGGRAPH Asia 2024 Conference Papers*, 2024, pp. 1–11.
- [53] H. Lu, G. Yang, N. Fei, Y. Huo, Z. Lu, P. Luo, and M. Ding, "Vdt: General-purpose video diffusion transformers via mask modeling," *arXiv*, 2023.
- [54] A. Gupta, L. Yu, K. Sohn, X. Gu, M. Hahn, F.-F. Li, I. Essa, L. Jiang, and J. Lezama, "Photorealistic video generation with diffusion models," in *European Conference on Computer Vision*. Springer, 2024, pp. 393–411.
- [55] S. Chen, M. Xu, J. Ren, Y. Cong, S. He, Y. Xie, A. Sinha, P. Luo, T. Xiang, and J.-M. Perez-Rua, "Gentron: Diffusion transformers for image and video generation," in *CVPR*, 2024, pp. 6441–6451.
- [56] P. Gao, L. Zhuo, Z. Lin, C. Liu, J. Chen, R. Du, E. Xie, X. Luo, L. Qiu, Y. Zhang *et al.*, "Lumina-t2x: Transforming text into any modality, resolution, and duration via flow-based large diffusion transformers," *arXiv*, 2024.
- [57] Z. Yang, J. Teng, W. Zheng, M. Ding, S. Huang, J. Xu, Y. Yang, W. Hong, X. Zhang, G. Feng *et al.*, "Cogvideox: Text-to-video diffusion models with an expert transformer," *arXiv*, 2024.
- [58] N. Agarwal, A. Ali, M. Bala, Y. Balaji, E. Barker, T. Cai, P. Chatopadhyay, Y. Chen, Y. Cui, Y. Ding *et al.*, "Cosmos world foundation model platform for physical ai," *arXiv*, 2025.
- [59] L. Yu, Y. Cheng, K. Sohn, J. Lezama, H. Zhang, H. Chang, A. G. Hauptmann, M.-H. Yang, Y. Hao, I. Essa *et al.*, "Magvit: Masked generative video transformer," in *CVPR*, 2023, pp. 10 459–10 469.
- [60] W. Hong, M. Ding, W. Zheng, X. Liu, and J. Tang, "Cogvideo: Large-scale pretraining for text-to-video generation via transformers," *arXiv*, 2022.
- [61] D. Kondratyuk, L. Yu, X. Gu, J. Lezama, J. Huang, R. Hornung, H. Adam, H. Akbari, Y. Alon, V. Birodkar *et al.*, "Videopoet: A large language model for zero-shot video generation," *arXiv*, 2023.
- [62] J. Cho, F. D. Puspitasari, S. Zheng, J. Zheng, L.-H. Lee, T.-H. Kim, C. S. Hong, and C. Zhang, "Sora as an agi world model? a complete survey on text-to-video generation," *arXiv*, 2024.
- [63] A. Singh, "A survey of ai text-to-image and ai text-to-video generators," in *International Conference on Artificial Intelligence, Robotics and Control (AIRC)*, 2023, pp. 32–36.
- [64] A. Van Den Oord, O. Vinyals *et al.*, "Neural discrete representation learning," in *NeurIPS*, vol. 30, 2017.
- [65] W. Yan, Y. Zhang, P. Abbeel, and A. Srinivas, "Videogpt: Video generation using vq-vae and transformers," *arXiv*, 2021.
- [66] T. Karras, S. Laine, and T. Aila, "A style-based generator architecture for generative adversarial networks," in *CVPR*, 2019, pp. 4401–4410.
- [67] D. J. Zhang, J. Z. Wu, J.-W. Liu, R. Zhao, L. Ran, Y. Gu, D. Gao, and M. Z. Shou, "Show-1: Marrying pixel and latent diffusion models for text-to-video generation," *International Journal of Computer Vision*, pp. 1–15, 2024.
- [68] W. Peebles and S. Xie, "Scalable diffusion models with transformers," in *ICCV*, 2023, pp. 4195–4205.
- [69] W. Menapace, A. Siarohin, I. Skorokhodov, E. Deyneka, T.-S. Chen, A. Kag, Y. Fang, A. Stoliar, E. Ricci, J. Ren *et al.*, "Snap video: Scaled spatiotemporal transformers for text-to-video synthesis," in *CVPR*, 2024, pp. 7038–7048.
- [70] P. Esser, R. Rombach, and B. Ommer, "Taming transformers for high-resolution image synthesis," in *CVPR*, 2021, pp. 12 873–12 883.
- [71] L. Yu, J. Lezama, N. B. Gundavarapu, L. Versari, K. Sohn, D. Minnen, Y. Cheng, A. Gupta, X. Gu, A. G. Hauptmann *et al.*, "Language model beats diffusion-tokenizer is key to visual generation," *arXiv*, 2023.
- [72] Z. Luo, F. Shi, Y. Ge, Y. Yang, L. Wang, and Y. Shan, "Openmagvit2: An open-source project toward democratizing autoregressive visual generation," *arXiv*, 2024.
- [73] Y. Teng, H. Shi, X. Liu, X. Ning, G. Dai, Y. Wang, Z. Li, and X. Liu, "Accelerating autoregressive text-to-image generation with training-free speculative jacobi decoding," *arXiv*, 2024.
- [74] X. Wang, X. Zhang, Z. Luo, Q. Sun, Y. Cui, J. Wang, F. Zhang, Y. Wang, Z. Li, Q. Yu *et al.*, "Emu3: Next-token prediction is all you need," *arXiv*, 2024.
- [75] M. Ding, Z. Yang, W. Hong, W. Zheng, C. Zhou, D. Yin, J. Lin, X. Zou, Z. Shao, H. Yang *et al.*, "Cogview: Mastering text-to-image generation via transformers," *Advances in neural information processing systems*, vol. 34, pp. 19 822–19 835, 2021.

- [76] J. Z. Wu, Y. Ge, X. Wang, S. W. Lei, Y. Gu, Y. Shi, W. Hsu, Y. Shan, X. Qie, and M. Z. Shou, "Tune-a-video: One-shot tuning of image diffusion models for text-to-video generation," in *ICCV*, 2023, pp. 7623–7633.
- [77] X. Li, C. Ma, X. Yang, and M.-H. Yang, "Vidto: Video token merging for zero-shot video editing," in *CVPR*, 2024, pp. 7486–7495.
- [78] Z. Zhang, B. Li, X. Nie, C. Han, T. Guo, and L. Liu, "Towards consistent video editing with text-to-image diffusion models," in *NeurIPS*, vol. 36, 2024.
- [79] H. Jeong and J. C. Ye, "Ground-a-video: Zero-shot grounded video editing using text-to-image diffusion models," *arXiv*, 2023.
- [80] S. Liu, Y. Zhang, W. Li, Z. Lin, and J. Jia, "Video-p2p: Video editing with cross-attention control," in *CVPR*, 2024, pp. 8599–8608.
- [81] J. Bai, T. He, Y. Wang, J. Guo, H. Hu, Z. Liu, and J. Bian, "Uniedit: A unified tuning-free framework for video motion and appearance editing," *arXiv*, 2024.
- [82] M. Ku, C. Wei, W. Ren, H. Yang, and W. Chen, "Anyv2v: A plug-and-play framework for any video-to-video editing tasks," *arXiv*, 2024.
- [83] H. Ouyang, Q. Wang, Y. Xiao, Q. Bai, J. Zhang, K. Zheng, X. Zhou, Q. Chen, and Y. Shen, "Codef: Content deformation fields for temporally consistent video processing," in *CVPR*, 2024, pp. 8089–8099.
- [84] D. Ceylan, C.-H. P. Huang, and N. J. Mitra, "Pix2video: Video editing using image diffusion," in *ICCV*, 2023, pp. 23 206–23 217.
- [85] W. Yu, J. Xing, L. Yuan, W. Hu, X. Li, Z. Huang, X. Gao, T.-T. Wong, Y. Shan, and Y. Tian, "Viewcrafter: Taming video diffusion models for high-fidelity novel view synthesis," *arXiv*, 2024.
- [86] H. He, Y. Xu, Y. Guo, G. Wetzstein, B. Dai, H. Li, and C. Yang, "Cameractrl: Enabling camera control for text-to-video generation," *arXiv*, 2024.
- [87] J.-g. Kwak, E. Dong, Y. Jin, H. Ko, S. Mahajan, and K. M. Yi, "Vivid-1-to-3: Novel view synthesis with video diffusion models," in *CVPR*, 2024, pp. 6775–6785.
- [88] M. You, Z. Zhu, H. Liu, and J. Hou, "Nvs-solver: Video diffusion model as zero-shot novel view synthesizer," *arXiv*, 2024.
- [89] C. Chan, S. Ginosar, T. Zhou, and A. A. Efros, "Everybody dance now," in *ICCV*, 2019, pp. 5933–5942.
- [90] A. Siarohin, S. Lathuilière, S. Tulyakov, E. Ricci, and N. Sebe, "First order motion model for image animation," in *NeurIPS*, vol. 32, 2019.
- [91] L. Zhang, A. Rao, and M. Agrawala, "Adding conditional control to text-to-image diffusion models," in *ICCV*, 2023, pp. 3836–3847.
- [92] X. Ju, A. Zeng, C. Zhao, J. Wang, L. Zhang, and Q. Xu, "Humansd: A native skeleton-guided diffusion model for human image generation," in *ICCV*, 2023.
- [93] L. Hu, X. Gao, P. Zhang, K. Sun, B. Zhang, and L. Bo, "Animate anyone: Consistent and controllable image-to-video synthesis for character animation," *CVPR*, pp. 8153–8163, 2023.
- [94] B. Zhu, F. Wang, T. Lu, P. Liu, J. Su, J. Liu, Y. Zhang, Z. Wu, G.-J. Qi, and Y.-G. Jiang, "Zero-shot high-fidelity and pose-controllable character animation," *IJCAI*, 2024.
- [95] X. Wang, S. Zhang, C. Gao, J. Wang, X. Zhou, Y. Zhang, L. Yan, and N. Sang, "Unianimate: Taming unified video diffusion models for consistent human image animation," *arXiv*, 2024.
- [96] W. Liu, Z. Piao, J. Min, W. Luo, L. Ma, and S. Gao, "Liquid warping gan: A unified framework for human motion imitation, appearance transfer and novel view synthesis," in *ICCV*, 2019, pp. 5904–5913.
- [97] H.-I. Ho, L. Xue, J. Song, and O. Hilliges, "Learning locally editable virtual humans," in *CVPR*, 2023, pp. 21 024–21 035.
- [98] A. Eldesokey and P. Wonka, "Latentman: Generating consistent animated characters using image diffusion models," in *Proceedings of the IEEE/CVF Conference on Computer Vision and Pattern Recognition*, 2024, pp. 7510–7519.
- [99] Y. Men, Y. Yao, M. Cui, and B. Liefeng, "Mimo: Controllable character video synthesis with spatial decomposed modeling," *arXiv*, 2024.
- [100] A. Gupta, S. Watson, and H. Yin, "3d point cloud feature explanations using gradient-based methods," in *IJCNN*. IEEE, 2020, pp. 1–8.
- [101] A. Rossi, M. Barbiero, P. Scremin, and R. Carli, "Robust visibility surface determination in object space via plücker coordinates," *Journal of Imaging*, vol. 7, no. 6, p. 96, 2021.
- [102] B. Kerbl, G. Kopanas, T. Leimkühler, and G. Drettakis, "3d gaussian splatting for real-time radiance field rendering," *ACM TOG*, vol. 42, no. 4, 2023.
- [103] J. J. Park, P. Florence, J. Straub, R. Newcombe, and S. Lovegrove, "Deepsdf: Learning continuous signed distance functions for shape representation," in *CVPR*, 2019, pp. 165–174.
- [104] B. Mildenhall, P. P. Srinivasan, M. Tancik, J. T. Barron, R. Ramamoorthi, and R. Ng, "Nerf: Representing scenes as neural radiance fields for view synthesis," *Communications of the ACM*, vol. 65, no. 1, pp. 99–106, 2021.
- [105] T. Shen, J. Gao, K. Yin, M.-Y. Liu, and S. Fidler, "Deep marching tetrahedra: a hybrid representation for high-resolution 3d shape synthesis," in *NeurIPS*, 2021.
- [106] W. Liu, J. Sun, W. Li, T. Hu, and P. Wang, "Deep learning on point clouds and its application: A survey," *Sensors*, vol. 19, no. 19, p. 4188, 2019.
- [107] C. R. Qi, H. Su, K. Mo, and L. J. Guibas, "Pointnet: Deep learning on point sets for 3d classification and segmentation," in *CVPR*, 2017, pp. 652–660.
- [108] J. F. Blinn, "What is a pixel?" *IEEE Computer Graphics and Applications*, vol. 25, no. 5, pp. 82–87, 2005.
- [109] B. Mildenhall, P. P. Srinivasan, M. Tancik, J. T. Barron, R. Ramamoorthi, and R. Ng, "Nerf: Representing scenes as neural radiance fields for view synthesis," in *ECCV*, 2020, pp. 405–421.
- [110] S. Fridovich-Keil, A. Yu, M. Tancik, Q. Chen, B. Recht, and A. Kanazawa, "Plenoxels: Radiance fields without neural networks," in *CVPR*, 2022, pp. 5501–5510.
- [111] C. Sun, M. Sun, and H.-T. Chen, "Direct voxel grid optimization: Super-fast convergence for radiance fields reconstruction," in *CVPR*, 2022, pp. 5459–5469.
- [112] T. Müller, A. Evans, C. Schied, and A. Keller, "Instant neural graphics primitives with a multiresolution hash encoding," *ACM TOG*, vol. 41, no. 4, pp. 1–15, 2022.
- [113] E. R. Chan, C. Z. Lin, M. A. Chan, K. Nagano, B. Pan, S. De Mello, O. Gallo, L. J. Guibas, J. Tremblay, S. Khamis *et al.*, "Efficient geometry-aware 3d generative adversarial networks," in *CVPR*, 2022, pp. 16 123–16 133.
- [114] A. Nichol, H. Jun, P. Dhariwal, P. Mishkin, and M. Chen, "Point-e: A system for generating 3d point clouds from complex prompts," *arXiv*, 2022.
- [115] G. Nam, M. Khelifi, A. Rodriguez, A. Tono, L. Zhou, and P. Guerrero, "3d-ldm: Neural implicit 3d shape generation with latent diffusion models," *arXiv*, 2022.
- [116] J. Lorraine, K. Xie, X. Zeng, C.-H. Lin, T. Takikawa, N. Sharp, T.-Y. Lin, M.-Y. Liu, S. Fidler, and J. Lucas, "Att3d: Amortized text-to-3d object synthesis," in *ICCV*, 2023, pp. 17 946–17 956.
- [117] M. Li, Y. Duan, J. Zhou, and J. Lu, "Diffusion-sdf: Text-to-shape via voxelized diffusion," in *CVPR*, 2023, pp. 12 642–12 651.
- [118] K. Xie, J. Lorraine, T. Cao, J. Gao, J. Lucas, A. Torralba, S. Fidler, and X. Zeng, "Latte3d: Large-scale amortized text-to-enhanced3d synthesis," in *European Conference on Computer Vision*. Springer, 2024, pp. 305–322.
- [119] Z. Liu, Y. Feng, M. J. Black, D. Nowrouzezahrai, L. Paull, and W. Liu, "Meshdiffusion: Score-based generative 3d mesh modeling," in *ICLR*, 2023.
- [120] H. Jun and A. Nichol, "Shap-e: Generating conditional 3d implicit functions," *arXiv*, 2023.
- [121] S. Babu, R. Liu, A. Zhou, M. Maire, G. Shakhnarovich, and R. Hanocka, "Hyperfields: Towards zero-shot generation of nerfs from text," in *ICML*, 2024.
- [122] Z. Zhao, W. Liu, X. Chen, X. Zeng, R. Wang, P. Cheng, B. Fu, T. Chen, G. Yu, and S. Gao, "Michelangelo: Conditional 3d shape generation based on shape-image-text aligned latent representation," *Advances in neural information processing systems*, vol. 36, pp. 73 969–73 982, 2023.
- [123] G. Qian, J. Cao, A. Siarohin, Y. Kant, C. Wang, M. Vasilkovsky, H.-Y. Lee, Y. Fang, I. Skorokhodov, P. Zhuang *et al.*, "Atom: Amortized text-to-mesh using 2d diffusion," *arXiv*, 2024.
- [124] C.-H. Lin, J. Gao, L. Tang, T. Takikawa, X. Zeng, X. Huang, K. Kreis, S. Fidler, M.-Y. Liu, and T.-Y. Lin, "Magic3d: High-resolution text-to-3d content creation," in *CVPR*, 2023.
- [125] J. Xu, X. Wang, W. Cheng, Y.-P. Cao, Y. Shan, X. Qie, and S. Gao, "Dream3d: Zero-shot text-to-3d synthesis using 3d shape prior and text-to-image diffusion models," in *CVPR*, 2023, pp. 20 908–20 918.

- [126] R. Chen, Y. Chen, N. Jiao, and K. Jia, "Fantasia3d: Disentangling geometry and appearance for high-quality text-to-3d content creation," in *ICCV*, 2023, pp. 22 246–22 256.
- [127] B. Poole, A. Jain, J. T. Barron, and B. Mildenhall, "Dreamfusion: Text-to-3d using 2d diffusion," in *ICLR*, 2023.
- [128] Z. Wang, C. Lu, Y. Wang, F. Bao, C. Li, H. Su, and J. Zhu, "Prolificdreamer: High-fidelity and diverse text-to-3d generation with variational score distillation," in *NeurIPS*, vol. 36, 2023.
- [129] Y.-T. Liu, Y.-C. Guo, G. Luo, H. Sun, W. Yin, and S.-H. Zhang, "Pi3d: Efficient text-to-3d generation with pseudo-image diffusion," in *CVPR*, 2024, pp. 19 915–19 924.
- [130] Y. Chen, Y. Pan, H. Yang, T. Yao, and T. Mei, "Vp3d: Unleashing 2d visual prompt for text-to-3d generation," in *CVPR*, 2024, pp. 4896–4905.
- [131] Y. Shi, P. Wang, J. Ye, M. Long, K. Li, and X. Yang, "Mvdream: Multi-view diffusion for 3d generation," *arXiv*, 2023.
- [132] J. Tang, J. Ren, H. Zhou, Z. Liu, and G. Zeng, "Dreamgaussian: Generative gaussian splatting for efficient 3d content creation," in *ICLR*, 2024.
- [133] T. Yi, J. Fang, G. Wu, L. Xie, X. Zhang, W. Liu, Q. Tian, and X. Wang, "Gaussiandreamer: Fast generation from text to 3d gaussian splatting with point cloud priors," *arXiv*, 2023.
- [134] Z. Chen, F. Wang, Y. Wang, and H. Liu, "Text-to-3d using gaussian splatting," in *CVPR*, 2024, pp. 21 401–21 412.
- [135] C. Chen, X. Yang, F. Yang, C. Feng, Z. Fu, C.-S. Foo, G. Lin, and F. Liu, "Sculpt3d: Multi-view consistent text-to-3d generation with sparse 3d prior," in *CVPR*, 2024, pp. 10 228–10 237.
- [136] J. Li, H. Tan, K. Zhang, Z. Xu, F. Luan, Y. Xu, Y. Hong, K. Sunkavalli, G. Shakhnarovich, and S. Bi, "Instant3d: Fast text-to-3d with sparse-view generation and large reconstruction model," in *ICLR*, 2024.
- [137] Y. Lu, J. Zhang, S. Li, T. Fang, D. McKinnon, Y. Tsin, L. Quan, X. Cao, and Y. Yao, "Direct2.5: Diverse text-to-3d generation via multi-view 2.5 d diffusion," in *CVPR*, 2024, pp. 8744–8753.
- [138] F. Liu, D. Wu, Y. Wei, Y. Rao, and Y. Duan, "Sherpa3d: Boosting high-fidelity text-to-3d generation via coarse 3d prior," in *CVPR*, 2024, pp. 20 763–20 774.
- [139] A. Gupta, W. Xiong, Y. Nie, I. Jones, and B. Oğuz, "3dgen: Triplane latent diffusion for textured mesh generation," *arXiv*, 2023.
- [140] L. Zhang, Z. Wang, Q. Zhang, Q. Qiu, A. Pang, H. Jiang, W. Yang, L. Xu, and J. Yu, "Clay: A controllable large-scale generative model for creating high-quality 3d assets," *ACM TOG*, vol. 43, no. 4, pp. 1–20, 2024.
- [141] W. Li, J. Liu, R. Chen, Y. Liang, X. Chen, P. Tan, and X. Long, "Craftsman: High-fidelity mesh generation with 3d native generation and interactive geometry refiner," *arXiv*, 2024.
- [142] W. Shuang, Y. Lin, Y. Zeng, F. Zhang, J. Xu, P. Torr, X. Cao, and Y. Yao, "Direct3d: Scalable image-to-3d generation via 3d latent diffusion transformer," *Advances in Neural Information Processing Systems*, vol. 37, pp. 121 859–121 881, 2025.
- [143] J. Xiang, Z. Lv, S. Xu, Y. Deng, R. Wang, B. Zhang, D. Chen, X. Tong, and J. Yang, "Structured 3d latents for scalable and versatile 3d generation," *arXiv*, 2024.
- [144] L. Melas-Kyriazi, I. Laina, C. Rupprecht, and A. Vedaldi, "Real-fusion: 360deg reconstruction of any object from a single image," in *CVPR*, 2023, pp. 8446–8455.
- [145] R. Liu, R. Wu, B. Van Hoorick, P. Tokmakov, S. Zakharov, and C. Vondrick, "Zero-1-to-3: Zero-shot one image to 3d object," in *ICCV*, 2023, pp. 9298–9309.
- [146] G. Qian, J. Mai, A. Hamdi, J. Ren, A. Siarohin, B. Li, H.-Y. Lee, I. Skorokhodov, P. Wonka, S. Tulyakov *et al.*, "Magic123: One image to high-quality 3d object generation using both 2d and 3d diffusion priors," *arXiv*, 2023.
- [147] Y. Liu, C. Lin, Z. Zeng, X. Long, L. Liu, T. Komura, and W. Wang, "Syncdreamer: Generating multiview-consistent images from a single-view image," in *ICLR*, 2024.
- [148] H. Weng, T. Yang, J. Wang, Y. Li, T. Zhang, C. Chen, and L. Zhang, "Consistent123: Improve consistency for one image to 3d object synthesis," *arXiv*, 2023.
- [149] Y. Shi, J. Wang, H. Cao, B. Tang, X. Qi, T. Yang, Y. Huang, S. Liu, L. Zhang, and H.-Y. Shum, "Toss: High-quality text-guided novel view synthesis from a single image," *arXiv*, 2023.
- [150] P. Wang and Y. Shi, "Imagedream: Image-prompt multi-view diffusion for 3d generation," *arXiv*, 2023.
- [151] X. Long, Y.-C. Guo, C. Lin, Y. Liu, Z. Dou, L. Liu, Y. Ma, S.-H. Zhang, M. Habermann, C. Theobalt *et al.*, "Wonder3d: Single image to 3d using cross-domain diffusion," in *CVPR*, 2024, pp. 9970–9980.
- [152] M. Liu, C. Xu, H. Jin, L. Chen, M. Varma T, Z. Xu, and H. Su, "One-2-3-45: Any single image to 3d mesh in 45 seconds without per-shape optimization," in *NeurIPS*, vol. 36, 2023.
- [153] Z. Wang, Y. Wang, Y. Chen, C. Xiang, S. Chen, D. Yu, C. Li, H. Su, and J. Zhu, "Crm: Single image to 3d textured mesh with convolutional reconstruction model," in *European Conference on Computer Vision*. Springer, 2024, pp. 57–74.
- [154] J. Xu, W. Cheng, Y. Gao, X. Wang, S. Gao, and Y. Shan, "Instantmesh: Efficient 3d mesh generation from a single image with sparse-view large reconstruction models," *arXiv*, 2024.
- [155] Y. Hong, K. Zhang, J. Gu, S. Bi, Y. Zhou, D. Liu, F. Liu, K. Sunkavalli, T. Bui, and H. Tan, "Lrm: Large reconstruction model for single image to 3d," *arXiv*, 2023.
- [156] K. Wu, F. Liu, Z. Cai, R. Yan, H. Wang, Y. Hu, Y. Duan, and K. Ma, "Unique3d: High-quality and efficient 3d mesh generation from a single image," *arXiv*, 2024.
- [157] L. Melas-Kyriazi, I. Laina, C. Rupprecht, N. Neverova, A. Vedaldi, O. Gafni, and F. Kokkinos, "Im-3d: Iterative multi-view diffusion and reconstruction for high-quality 3d generation," *International Conference on Machine Learning*, 2024, 2024.
- [158] Z. Chen, Y. Wang, F. Wang, Z. Wang, and H. Liu, "V3d: Video diffusion models are effective 3d generators," *arXiv*, 2024.
- [159] V. Voleti, C.-H. Yao, M. Boss, A. Letts, D. Pankratz, D. Tochilkin, C. Laforge, R. Rombach, and V. Jampani, "Sv3d: Novel multi-view synthesis and 3d generation from a single image using latent video diffusion," in *European Conference on Computer Vision*. Springer, 2024, pp. 439–457.
- [160] R. Gao, A. Holynski, P. Henzler, A. Brussee, R. Martin-Brualla, P. Srinivasan, J. T. Barron, and B. Poole, "Cat3d: Create anything in 3d with multi-view diffusion models," *arXiv*, 2024.
- [161] X. Li, Q. Zhang, D. Kang, W. Cheng, Y. Gao, J. Zhang, Z. Liang, J. Liao, Y.-P. Cao, and Y. Shan, "Advances in 3d generation: A survey," *arXiv*, 2024.
- [162] C. Jiang, "A survey on text-to-3d contents generation in the wild," *arXiv*, 2024.
- [163] C. Li, C. Zhang, J. Cho, A. Waghvase, L.-H. Lee, F. Rameau, Y. Yang, S.-H. Bae, and C. S. Hong, "Generative ai meets 3d: A survey on text-to-3d in aigc era," *arXiv*, 2023.
- [164] A. Q. Nichol, P. Dhariwal, A. Ramesh, P. Shyam, P. Mishkin, B. McGrew, I. Sutskever, and M. Chen, "Glide: Towards photorealistic image generation and editing with text-guided diffusion models," in *ICML*, 2022, pp. 16 784–16 804.
- [165] T. Yi, J. Fang, J. Wang, G. Wu, L. Xie, X. Zhang, W. Liu, Q. Tian, and X. Wang, "Gaussiandreamer: Fast generation from text to 3d gaussians by bridging 2d and 3d diffusion models," in *CVPR*, 2024, pp. 6796–6807.
- [166] B. Zhang, J. Tang, M. Niessner, and P. Wonka, "3dshape2vecset: A 3d shape representation for neural fields and generative diffusion models," *ACM TOG*, vol. 42, no. 4, pp. 1–16, 2023.
- [167] M. Deitke, D. Schwenk, J. Salvador, L. Weihs, O. Michel, E. VanderBilt, L. Schmidt, K. Ehsani, A. Kembhavi, and A. Farhadi, "Objaverse: A universe of annotated 3d objects," in *CVPR*, 2023, pp. 13 142–13 153.
- [168] M. Deitke, R. Liu, M. Wallingford, H. Ngo, O. Michel, A. Kusupati, A. Fan, C. Laforge, V. Voleti, S. Y. Gadre *et al.*, "Objaverse-xl: A universe of 10m+ 3d objects," in *NeurIPS*, vol. 36, 2024.
- [169] C. Schuhmann, R. Beaumont, R. Vencu, C. Gordon, R. Wightman, M. Cherti, T. Coombes, A. Katta, C. Mullis, M. Wortsman *et al.*, "Laion-5b: An open large-scale dataset for training next generation image-text models," in *NeurIPS*, vol. 35, 2022, pp. 25 278–25 294.
- [170] T.-S. Chen, A. Siarohin, W. Menapace, E. Deyneka, H.-w. Chao, B. E. Jeon, Y. Fang, H.-Y. Lee, J. Ren, M.-H. Yang *et al.*, "Panda-70m: Captioning 70m videos with multiple cross-modality teachers," in *CVPR*, 2024, pp. 13 320–13 331.
- [171] H. Wang, X. Du, J. Li, R. A. Yeh, and G. Shakhnarovich, "Score jacobian chaining: Lifting pretrained 2d diffusion models for 3d generation," in *CVPR*, 2023, pp. 12 619–12 629.
- [172] Y. Li, X. Liu, A. Kag, J. Hu, Y. Idelbayev, D. Sagar, Y. Wang, S. Tulyakov, and J. Ren, "Textcraftor: Your text encoder can be image quality controller," in *CVPR*, 2024, pp. 7985–7995.
- [173] X. Liu, Q. Wu, H. Zhou, Y. Xu, R. Qian, X. Lin, X. Zhou, W. Wu, B. Dai, and B. Zhou, "Learning hierarchical cross-modal association for co-speech gesture generation," in *CVPR*, 2022, pp. 10 462–10 472.



- [174] Y. Du, X. Liu, S. Liu, J. Zhang, and B. Zhou, "Chemspace: Toward steerable and interpretable chemical space exploration," *Transactions on Machine Learning Research*, 2022.
- [175] L. Zhu, X. Liu, X. Liu, R. Qian, Z. Liu, and L. Yu, "Taming diffusion models for audio-driven co-speech gesture generation," in *CVPR*, 2023, pp. 10544–10553.
- [176] Q. Wu, X. Liu, Y. Chen, K. Li, C. Zheng, J. Cai, and J. Zheng, "Object-compositional neural implicit surfaces," in *ECCV*, 2022, pp. 197–213.
- [177] X. Liu, Q. Wu, H. Zhou, Y. Du, W. Wu, D. Lin, and Z. Liu, "Audio-driven co-speech gesture video generation," in *NeurIPS*, vol. 35, 2022, pp. 21386–21399.
- [178] K. Sun, K. Huang, X. Liu, Y. Wu, Z. Xu, Z. Li, and X. Liu, "T2v-compench: A comprehensive benchmark for compositional text-to-video generation," *arXiv*, 2024.
- [179] X. Liu, Y. Xu, Q. Wu, H. Zhou, W. Wu, and B. Zhou, "Semantic-aware implicit neural audio-driven video portrait generation," in *ECCV*, 2022, pp. 106–125.
- [180] Z. Yu, W. Cheng, X. Liu, W. Wu, and K.-Y. Lin, "Monohuman: Animatable human neural field from monocular video," in *CVPR*, 2023, pp. 16943–16953.
- [181] X. Liu, R. Qian, H. Zhou, D. Hu, W. Lin, Z. Liu, B. Zhou, and X. Zhou, "Visual sound localization in the wild by cross-modal interference erasing," in *AAAI*, vol. 36, no. 2, 2022, pp. 1801–1809.
- [182] E. J. Hu, Y. Shen, P. Wallis, Z. Allen-Zhu, Y. Li, S. Wang, L. Wang, and W. Chen, "Lora: Low-rank adaptation of large language models," *arXiv*, 2021.
- [183] Z. Wang, Z. Yuan, X. Wang, Y. Li, T. Chen, M. Xia, P. Luo, and Y. Shan, "Motionctrl: A unified and flexible motion controller for video generation," in *SIGGRAPH*, 2024, pp. 1–11.
- [184] A. Blattmann, T. Dockhorn, S. Kulal, D. Mendelevitch, M. Kilian, D. Lorenz, Y. Levi, Z. English, V. Voleti, A. Letts *et al.*, "Stable video diffusion: Scaling latent video diffusion models to large datasets," *arXiv*, 2023.
- [185] R. Zhao, W. Li, Z. Hu, L. Li, Z. Zou, Z. Shi, and C. Fan, "Zero-shot text-to-parameter translation for game character auto-creation," in *CVPR*, 2023, pp. 21013–21023.
- [186] L. Zhang, Q. Qiu, H. Lin, Q. Zhang, C. Shi, W. Yang, Y. Shi, S. Yang, L. Xu, and J. Yu, "Dreamface: Progressive generation of animatable 3d faces under text guidance," *arXiv*, 2023.
- [187] X. Han, Y. Cao, K. Han, X. Zhu, J. Deng, Y.-Z. Song, T. Xiang, and K.-Y. K. Wong, "Headsulpt: Crafting 3d head avatars with text," in *NeurIPS*, vol. 36, 2023.
- [188] N. Kolotouros, T. Alldieck, A. Zanfir, E. Bazavan, M. Fieraru, and C. Sminchisescu, "Dreamhuman: Animatable 3d avatars from text," in *NeurIPS*, vol. 36, 2023.
- [189] Y. Huang, J. Wang, A. Zeng, H. Cao, X. Qi, Y. Shi, Z.-J. Zha, and L. Zhang, "Dreamwaltz: Make a scene with complex 3d animatable avatars," in *NeurIPS*, vol. 36, 2023.
- [190] G. Tevet, B. Gordon, A. Hertz, A. H. Bermano, and D. Cohen-Or, "Motionclip: Exposing human motion generation to clip space," in *ECCV*, 2022, pp. 358–374.
- [191] S. Tu, Q. Dai, Z.-Q. Cheng, H. Hu, X. Han, Z. Wu, and Y.-G. Jiang, "Motioneditor: Editing video motion via content-aware diffusion," in *CVPR*, 2024, pp. 7882–7891.
- [192] L. Song, L. Cao, H. Xu, K. Kang, F. Tang, J. Yuan, and Y. Zhao, "Roomdreamer: Text-driven 3d indoor scene synthesis with coherent geometry and texture," *arXiv*, 2023.
- [193] J. Zhang, X. Li, Z. Wan, C. Wang, and J. Liao, "Text2nerf: Text-driven 3d scene generation with neural radiance fields," *IEEE Transactions on Visualization and Computer Graphics*, 2024.
- [194] H. Li, H. Shi, W. Zhang, W. Wu, Y. Liao, L. Wang, L.-h. Lee, and P. Y. Zhou, "Dreamscene: 3d gaussian-based text-to-3d scene generation via formation pattern sampling," in *European Conference on Computer Vision*. Springer, 2024, pp. 214–230.
- [195] F. Lu, K.-Y. Lin, Y. Xu, H. Li, G. Chen, and C. Jiang, "Urban architect: Steerable 3d urban scene generation with layout prior," *arXiv*, 2024.
- [196] S. Zhou, Z. Fan, D. Xu, H. Chang, P. Chari, T. Bharadwaj, S. You, Z. Wang, and A. Kadambi, "Dreamscene360: Unconstrained text-to-3d scene generation with panoramic gaussian splatting," in *ECCV*, 2024, pp. 324–342.
- [197] J. Deng, W. Chai, J. Huang, Z. Zhao, Q. Huang, M. Gao, J. Guo, S. Hao, W. Hu, J.-N. Hwang *et al.*, "Citycraft: A real crafter for 3d city generation," *arXiv*, 2024.
- [198] W. Gao, N. Aigerman, T. Groueix, V. Kim, and R. Hanocka, "Textdeformer: Geometry manipulation using text guidance," in *SIGGRAPH*, 2023, pp. 1–11.
- [199] A. Haque, M. Tancik, A. A. Efros, A. Holynski, and A. Kanazawa, "Instruct-nerf2nerf: Editing 3d scenes with instructions," in *ICCV*, 2023, pp. 19740–19750.
- [200] Z. Fan, Y. Jiang, P. Wang, X. Gong, D. Xu, and Z. Wang, "Unified implicit neural stylization," in *ECCV*, 2022, pp. 636–654.
- [201] K. Zhang, N. Kolkin, S. Bi, F. Luan, Z. Xu, E. Shechtman, and N. Snavely, "Arf: Artistic radiance fields," in *ECCV*, 2022, pp. 717–733.
- [202] J. Sun, X. Wang, Y. Zhang, X. Li, Q. Zhang, Y. Liu, and J. Wang, "Fenerf: Face editing in neural radiance fields," in *CVPR*, 2022, pp. 7672–7682.
- [203] J. Zhang, X. Li, Z. Wan, C. Wang, and J. Liao, "Fdnerf: Few-shot dynamic neural radiance fields for face reconstruction and expression editing," in *SIGGRAPH Asia*, 2022, pp. 1–9.
- [204] Y. Peng, Y. Yan, S. Liu, Y. Cheng, S. Guan, B. Pan, G. Zhai, and X. Yang, "Cagenerf: Cage-based neural radiance field for generalized 3d deformation and animation," in *NeurIPS*, vol. 35, 2022, pp. 31402–31415.
- [205] W.-C. Tseng, H.-J. Liao, L. Yen-Chen, and M. Sun, "Cla-nerf: Category-level articulated neural radiance field," in *ICRA*, 2022, pp. 8454–8460.
- [206] S. Kobayashi, E. Matsumoto, and V. Sitzmann, "Decomposing nerf for editing via feature field distillation," in *NeurIPS*, vol. 35, 2022, pp. 23311–23330.
- [207] Q. Wu, K. Wang, K. Li, J. Zheng, and J. Cai, "Objectsdf++: Improved object-compositional neural implicit surfaces," in *ICCV*, 2023, pp. 21764–21774.
- [208] J. Tang, Z. Li, Z. Hao, X. Liu, G. Zeng, M.-Y. Liu, and Q. Zhang, "Edgerunner: Auto-regressive auto-encoder for artistic mesh generation," *arXiv*, 2024.
- [209] X. Liu, X. Zhan, J. Tang, Y. Shan, G. Zeng, D. Lin, X. Liu, and Z. Liu, "Humangaussian: Text-driven 3d human generation with gaussian splatting," in *CVPR*, 2024, pp. 6646–6657.
- [210] R. Shao, J. Sun, C. Peng, Z. Zheng, B. Zhou, H. Zhang, and Y. Liu, "Control4d: Efficient 4d portrait editing with text," in *CVPR*, 2024, pp. 4556–4567.
- [211] Y. Jiang, C. Yu, C. Cao, F. Wang, W. Hu, and J. Gao, "Animate3d: Animating any 3d model with multi-view video diffusion," *Advances in Neural Information Processing Systems*, vol. 37, pp. 125879–125906, 2025.
- [212] Y. Wang, X. Wang, Z. Chen, Z. Wang, F. Sun, and J. Zhu, "Vidu4d: Single generated video to high-fidelity 4d reconstruction with dynamic gaussian surfels," *Advances in Neural Information Processing Systems*, vol. 37, pp. 131316–131343, 2025.
- [213] H. Liang, Y. Yin, D. Xu, H. Liang, Z. Wang, K. N. Plataniotis, Y. Zhao, and Y. Wei, "Diffusion4d: Fast spatial-temporal consistent 4d generation via video diffusion models," *NeurIPS*, 2024.
- [214] J. Ren, K. Xie, A. Mirzaei, H. Liang, X. Zeng, K. Kreis, Z. Liu, A. Torralba, S. Fidler, S. W. Kim, and H. Ling, "L4gm: Large 4d gaussian reconstruction model," in *NeurIPS*, 2024.
- [215] U. Singer, S. Sheynin, A. Polyak, O. Ashual, I. Makarov, F. Kokkinos, N. Goyal, A. Vedaldi, D. Parikh, J. Johnson *et al.*, "Text-to-4d dynamic scene generation," *arXiv*, 2023.
- [216] S. Bahmani, I. Skorokhodov, V. Rong, G. Wetzstein, L. Guibas, P. Wonka, S. Tulyakov, J. J. Park, A. Tagliasacchi, and D. B. Lindell, "4d-fy: Text-to-4d generation using hybrid score distillation sampling," in *CVPR*, 2024.
- [217] H. Ling, S. W. Kim, A. Torralba, S. Fidler, and K. Kreis, "Align your gaussians: Text-to-4d with dynamic 3d gaussians and composed diffusion models," in *CVPR*, 2024, pp. 8576–8588.
- [218] X. Yu, Y.-C. Guo, Y. Li, D. Liang, S.-H. Zhang, and X. Qi, "Text-to-3d with classifier score distillation," *arXiv*, 2023.
- [219] Y. Zheng, X. Li, K. Nagano, S. Liu, O. Hilliges, and S. D. Mello, "A unified approach for text- and image-guided 4d scene generation," in *CVPR*, 2024.
- [220] S. Bahmani, X. Liu, W. Yifan, I. Skorokhodov, V. Rong, Z. Liu, X. Liu, J. J. Park, S. Tulyakov, G. Wetzstein *et al.*, "Tc4d: Trajectory-conditioned text-to-4d generation," in *ECCV*, 2024, pp. 53–72.
- [221] H. Yu, C. Wang, P. Zhuang, W. Menapace, A. Siarohin, J. Cao, L. A. Jeni, S. Tulyakov, and H.-Y. Lee, "dreal: Towards photorealistic 4d scene generation via video diffusion models," *NeurIPS*, 2024.

- [222] H. Zhu, T. He, A. Tang, J. Guo, Z. Chen, and J. Bian, "Compositional 3d-aware video generation with llm director," *NeurIPS*, 2024.
- [223] Y. Jiang, L. Zhang, J. Gao, W. Hu, and Y. Yao, "Consistent4d: Consistent 360° dynamic object generation from monocular video," *arXiv*, 2023.
- [224] Z. Wu, C. Yu, Y. Jiang, C. Cao, F. Wang, and X. Bai, "Sc4d: Sparse-controlled video-to-4d generation and motion transfer," in *ECCV*, 2024, pp. 361–379.
- [225] Y.-H. Huang, Y.-T. Sun, Z. Yang, X. Lyu, Y.-P. Cao, and X. Qi, "Sc-gs: Sparse-controlled gaussian splatting for editable dynamic scenes," in *CVPR*, 2024, pp. 4220–4230.
- [226] Y. Zeng, Y. Jiang, S. Zhu, Y. Lu, Y. Lin, H. Zhu, W. Hu, X. Cao, and Y. Yao, "Stag4d: Spatial-temporal anchored generative 4d gaussians," in *ECCV*, 2025, pp. 163–179.
- [227] W.-H. Chu, L. Ke, and K. Fragkiadaki, "Dreamscene4d: Dynamic multi-object scene generation from monocular videos," *arXiv*, 2024.
- [228] H. Zhang, X. Chen, Y. Wang, X. Liu, Y. Wang, and Y. Qiao, "4diffusion: Multi-view video diffusion model for 4d generation," *arXiv*, 2024.
- [229] Z. Li, Y. Chen, and P. Liu, "Dreammesh4d: Video-to-4d generation with sparse-controlled gaussian-mesh hybrid representation," in *NeurIPS*, 2024.
- [230] W. Xian, J.-B. Huang, J. Kopf, and C. Kim, "Space-time neural irradiance fields for free-viewpoint video," in *CVPR*, 2021, pp. 9421–9431.
- [231] C. Gao, A. Saraf, J. Kopf, and J.-B. Huang, "Dynamic view synthesis from dynamic monocular video," in *ICCV*, 2021, pp. 5712–5721.
- [232] T. Li, M. Slavcheva, M. Zollhoefer, S. Green, C. Lassner, C. Kim, T. Schmidt, S. Lovegrove, M. Goesele, R. Newcombe *et al.*, "Neural 3d video synthesis from multi-view video," in *CVPR*, 2022, pp. 5521–5531.
- [233] Z. Li, S. Niklaus, N. Snavely, and O. Wang, "Neural scene flow fields for space-time view synthesis of dynamic scenes," in *CVPR*, 2021, pp. 6498–6508.
- [234] A. Cao and J. Johnson, "Hexplane: A fast representation for dynamic scenes," in *CVPR*, 2023, pp. 130–141.
- [235] S. Fridovich-Keil, G. Meanti, F. R. Warburg, B. Recht, and A. Kanazawa, "K-planes: Explicit radiance fields in space, time, and appearance," in *CVPR*, 2023, pp. 12 479–12 488.
- [236] R. Shao, Z. Zheng, H. Tu, B. Liu, H. Zhang, and Y. Liu, "Tensor4d: Efficient neural 4d decomposition for high-fidelity dynamic reconstruction and rendering," in *CVPR*, 2023, pp. 16 632–16 642.
- [237] H. Turki, J. Y. Zhang, F. Ferroni, and D. Ramanan, "Suds: Scalable urban dynamic scenes," in *CVPR*, 2023, pp. 12 375–12 385.
- [238] J. Luiten, G. Kopanas, B. Leibe, and D. Ramanan, "Dynamic 3d gaussians: Tracking by persistent dynamic view synthesis," in *2024 International Conference on 3D Vision (3DV)*. IEEE, 2024, pp. 800–809.
- [239] A. Pumarola, E. Corona, G. Pons-Moll, and F. Moreno-Noguer, "D-nerf: Neural radiance fields for dynamic scenes," in *CVPR*, 2021, pp. 10 318–10 327.
- [240] X. Li, Z. Cao, H. Sun, J. Zhang, K. Xian, and G. Lin, "3d cinematography from a single image," in *CVPR*, 2023, pp. 4595–4605.
- [241] G. Wu, T. Yi, J. Fang, L. Xie, X. Zhang, W. Wei, W. Liu, Q. Tian, and X. Wang, "4d gaussian splatting for real-time dynamic scene rendering," in *CVPR*, 2024, pp. 20 310–20 320.
- [242] V. Ordonez, G. Kulkarni, and T. Berg, "Im2text: Describing images using 1 million captioned photographs," in *NeurIPS*, vol. 24, 2011.
- [243] T.-Y. Lin, M. Maire, S. Belongie, J. Hays, P. Perona, D. Ramanan, P. Dollár, and C. L. Zitnick, "Microsoft coco: Common objects in context," in *ECCV*, 2014, pp. 740–755.
- [244] P. Sharma, N. Ding, S. Goodman, and R. Soricut, "Conceptual captions: A cleaned, hypertexted, image alt-text dataset for automatic image captioning," in *ACL*, 2018, pp. 2556–2565.
- [245] L. Chen, J. Li, X. Dong, P. Zhang, C. He, J. Wang, F. Zhao, and D. Lin, "Sharegpt4v: Improving large multi-modal models with better captions," in *ECCV*, 2025, pp. 370–387.
- [246] Y. Kirstain, A. Polyak, U. Singer, S. Matiana, J. Penna, and O. Levy, "Pick-a-pic: An open dataset of user preferences for text-to-image generation," in *NeurIPS*, vol. 36, 2023, pp. 36 652–36 663.
- [247] K. Soomro, "Ucf101: A dataset of 101 human actions classes from videos in the wild," *arXiv*, 2012.
- [248] F. Caba Heilbron, V. Escorcia, B. Ghanem, and J. Carlos Nieves, "Activitynet: A large-scale video benchmark for human activity understanding," in *CVPR*, 2015, pp. 961–970.
- [249] J. Xu, T. Mei, T. Yao, and Y. Rui, "Msr-vtt: A large video description dataset for bridging video and language," in *CVPR*, 2016, pp. 5288–5296.
- [250] A. Miech, D. Zhukov, J.-B. Alayrac, M. Tapaswi, I. Laptev, and J. Sivic, "Howto100m: Learning a text-video embedding by watching hundred million narrated video clips," in *ICCV*, 2019, pp. 2630–2640.
- [251] M. Bain, A. Nagrani, G. Varol, and A. Zisserman, "Frozen in time: A joint video and image encoder for end-to-end retrieval," in *ICCV*, 2021, pp. 1728–1738.
- [252] H. Xue, T. Hang, Y. Zeng, Y. Sun, B. Liu, H. Yang, J. Fu, and B. Guo, "Advancing high-resolution video-language representation with large-scale video transcriptions," in *CVPR*, 2022.
- [253] Y. Wang, Y. He, Y. Li, K. Li, J. Yu, X. Ma, X. Li, G. Chen, X. Chen, Y. Wang *et al.*, "Internvid: A large-scale video-text dataset for multimodal understanding and generation," *arXiv*, 2023.
- [254] Q. Wang, Y. Shi, J. Ou, R. Chen, K. Lin, J. Wang, B. Jiang, H. Yang, M. Zheng, X. Tao *et al.*, "Koala-36m: A large-scale video dataset improving consistency between fine-grained conditions and video content," *arXiv*, 2024.
- [255] Z. Liu, P. Luo, S. Qiu, X. Wang, and X. Tang, "Deepfashion: Powering robust clothes recognition and retrieval with rich annotations," in *CVPR*, 2016, pp. 1096–1104.
- [256] J. Fu, S. Li, Y. Jiang, K.-Y. Lin, C. Qian, C. C. Loy, W. Wu, and Z. Liu, "Stylegan-human: A data-centric odyssey of human generation," in *ECCV*, 2022, pp. 1–19.
- [257] J. Reizenstein, R. Shapovalov, P. Henzler, L. Sbordone, P. Labatut, and D. Novotny, "Common objects in 3d: Large-scale learning and evaluation of real-life 3d category reconstruction," in *ICCV*, 2021, pp. 10 901–10 911.
- [258] J. Tremblay, M. Meshry, A. Evans, J. Kautz, A. Keller, S. Khamis, C. Loop, N. Morrical, K. Nagano, T. Takikawa *et al.*, "Rtmv: A ray-traced multi-view synthetic dataset for novel view synthesis. iee," in *CVF European Conference on Computer Vision Workshop (Learn3DG ECCVW)*, vol. 2022, no. 2, 2022, p. 5.
- [259] X. Yu, M. Xu, Y. Zhang, H. Liu, C. Ye, Y. Wu, Z. Yan, C. Zhu, Z. Xiong, T. Liang *et al.*, "Mvimgnet: A large-scale dataset of multi-view images," in *CVPR*, 2023, pp. 9150–9161.
- [260] X. Liu, P. Tayal, J. Wang, J. Zarzar, T. Monnier, K. Tertikas, J. Duan, A. Tsoisou, J. Y. Zhang, N. Neverova, A. Vedaldi, R. Shapovalov, and D. Novotny, "Uncommon objects in 3d," *arXiv*, 2025.
- [261] A. X. Chang, T. Funkhouser, L. Guibas, P. Hanrahan, Q. Huang, Z. Li, S. Savarese, M. Savva, S. Song, H. Su *et al.*, "Shapenet: An information-rich 3d model repository," *arXiv*, 2015.
- [262] H. Fu, R. Jia, L. Gao, M. Gong, B. Zhao, S. Maybank, and D. Tao, "3d-future: 3d furniture shape with texture," *International Journal of Computer Vision*, vol. 129, pp. 3313–3337, 2021.
- [263] L. Downs, A. Francis, N. Koenig, B. Kinman, R. Hickman, K. Reymann, T. B. McHugh, and V. Vanhoucke, "Google scanned objects: A high-quality dataset of 3d scanned household items," in *ICRA*, 2022, pp. 2553–2560.
- [264] T. Luo, C. Rockwell, H. Lee, and J. Johnson, "Scalable 3d captioning with pretrained models," in *NeurIPS*, vol. 36, 2024.
- [265] K. Ataallah, X. Shen, E. Abdelrahman, E. Sleiman, D. Zhu, J. Ding, and M. Elhoseiny, "Minigpt4-video: Advancing multimodal llms for video understanding with interleaved visual-textual tokens," *arXiv*, 2024.
- [266] Y. Zhao, C.-C. Lin, K. Lin, Z. Yan, L. Li, Z. Yang, J. Wang, G. H. Lee, and L. Wang, "Genxd: Generating any 3d and 4d scenes," *arXiv*, 2024.
- [267] W. Wang, H.-I. Ho, C. Guo, B. Rong, A. Grigorev, J. Song, J. J. Zarate, and O. Hilliges, "4d-dress: A 4d dataset of real-world human clothing with semantic annotations," in *CVPR*, 2024, pp. 550–560.
- [268] Z. Wang, A. C. Bovik, H. R. Sheikh, and E. P. Simoncelli, "Image quality assessment: from error visibility to structural similarity," *IEEE transactions on image processing*, vol. 13, no. 4, pp. 600–612, 2004.
- [269] R. Zhang, P. Isola, A. A. Efros, E. Shechtman, and O. Wang, "The unreasonable effectiveness of deep features as a perceptual metric," in *CVPR*, 2018.
- [270] M. Heusel, H. Ramsauer, T. Unterthiner, B. Nessler, and S. Hochreiter, "Gans trained by a two time-scale update rule converge to a local nash equilibrium," in *NeurIPS*, vol. 30, 2017.

- [271] T. Salimans, I. Goodfellow, W. Zaremba, V. Cheung, A. Radford, and X. Chen, "Improved techniques for training gans," in *NeurIPS*, vol. 29, 2016.
- [272] T. Unterthiner, S. van Steenkiste, K. Kurach, R. Marinier, M. Michalski, and S. Gelly, "Fvd: A new metric for video generation," in *ICLR Workshop*, 2019.
- [273] M. Saito, S. Saito, M. Koyama, and S. Kobayashi, "Train sparsely, generate densely: Memory-efficient unsupervised training of high-resolution temporal gan," *International Journal of Computer Vision*, vol. 128, no. 10, pp. 2586–2606, 2020.
- [274] D. Tran, L. Bourdev, R. Fergus, L. Torresani, and M. Paluri, "Learning spatiotemporal features with 3d convolutional networks," in *ICCV*, 2015, pp. 4489–4497.
- [275] J. Liu, Y. Qu, Q. Yan, X. Zeng, L. Wang, and R. Liao, "Fr'echet video motion distance: A metric for evaluating motion consistency in videos," *arXiv*, 2024.
- [276] J. Hessel, A. Holtzman, M. Forbes, R. L. Bras, and Y. Choi, "Clip-score: A reference-free evaluation metric for image captioning," *arXiv*, 2021.
- [277] D. H. Park, S. Azadi, X. Liu, T. Darrell, and A. Rohrbach, "Benchmark for compositional text-to-image synthesis," in *Thirty-fifth Conference on Neural Information Processing Systems Datasets and Benchmarks Track*, 2021.
- [278] B. Ni, H. Peng, M. Chen, S. Zhang, G. Meng, J. Fu, S. Xiang, and H. Ling, "Expanding language-image pretrained models for general video recognition," in *ECCV*, 2022, pp. 1–18.
- [279] A. Dosovitskiy, "An image is worth 16x16 words: Transformers for image recognition at scale," *arXiv*, 2020.
- [280] M. Caron, H. Touvron, I. Misra, H. Jégou, J. Mairal, P. Bojanowski, and A. Joulin, "Emerging properties in self-supervised vision transformers," in *ICCV*, 2021, pp. 9650–9660.
- [281] T. Brooks, A. Holynski, and A. A. Efros, "Instructpix2pix: Learning to follow image editing instructions," in *CVPR*, 2023, pp. 18392–18402.
- [282] L. Mou, J.-K. Chen, and Y.-X. Wang, "Instruct 4D-to-4D: Editing 4d scenes as pseudo-3d scenes using 2d diffusion," in *CVPR*, 2024.
- [283] M. Loper, N. Mahmood, J. Romero, G. Pons-Moll, and M. J. Black, "Smpl: A skinned multi-person linear model," in *Seminal Graphics Papers: Pushing the Boundaries, Volume 2*, 2023, pp. 851–866.
- [284] G. Pavlakos, V. Choutas, N. Ghorbani, T. Bolkart, A. A. Osman, D. Tzionas, and M. J. Black, "Expressive body capture: 3d hands, face, and body from a single image," in *CVPR*, 2019, pp. 10975–10985.
- [285] F. G. Harvey, M. Yurick, D. Nowrouzezahrai, and C. Pal, "Robust motion in-betweening," *ACM TOG*, vol. 39, no. 4, pp. 60–1, 2020.
- [286] P. Starke, S. Starke, T. Komura, and F. Steinicke, "Motion in-betweening with phase manifolds," *Proceedings of the ACM on Computer Graphics and Interactive Techniques*, vol. 6, no. 3, pp. 1–17, 2023.
- [287] J. Martinez, M. J. Black, and J. Romero, "On human motion prediction using recurrent neural networks," in *CVPR*, 2017, pp. 2891–2900.
- [288] Y. Tang, L. Ma, W. Liu, and W.-S. Zheng, "Long-term human motion prediction by modeling motion context and enhancing motion dynamic," in *IJCAI*, 2018.
- [289] E. Corona, A. Pumarola, G. Alenya, and F. Moreno-Noguer, "Context-aware human motion prediction," in *CVPR*, 2020.
- [290] T. Sofianos, A. Sampieri, L. Franco, and F. Galasso, "Space-time-separable graph convolutional network for pose forecasting," in *ICCV*, 2021.
- [291] X. Yan, A. Rastogi, R. Villegas, K. Sunkavalli, E. Shechtman, S. Hadap, E. Yumer, and H. Lee, "Mt-vae: Learning motion transformations to generate multimodal human dynamics," in *ECCV*, 2018, pp. 265–281.
- [292] J. Walker, K. Marino, A. Gupta, and M. Hebert, "The pose knows: Video forecasting by generating pose futures," in *ICCV*, 2017, pp. 3332–3341.
- [293] Y. Yuan and K. Kitani, "Dlow: Diversifying latent flows for diverse human motion prediction," in *ECCV*, 2020, pp. 346–364.
- [294] E. Barsoum, J. Kender, and Z. Liu, "Hp-gan: Probabilistic 3d human motion prediction via gan," in *CVPRW*, 2018, pp. 1418–1427.
- [295] W. Mao, M. Liu, and M. Salzmann, "Generating smooth pose sequences for diverse human motion prediction," in *ICCV*, 2021, pp. 13309–13318.
- [296] C. Guo, S. Zou, X. Zuo, S. Wang, W. Ji, X. Li, and L. Cheng, "Generating diverse and natural 3d human motions from text," in *CVPR*, 2022, pp. 5152–5161.
- [297] J. Zhang, Y. Zhang, X. Cun, Y. Zhang, H. Zhao, H. Lu, X. Shen, and Y. Shan, "T2m-gpt: Generating human motion from textual descriptions with discrete representations," in *CVPR*, 2023, pp. 14730–14740.
- [298] S. Lu, L.-H. Chen, A. Zeng, J. Lin, R. Zhang, L. Zhang, and H.-Y. Shum, "Humantomato: Text-aligned whole-body motion generation," in *ICML*, 2024.
- [299] B. Jiang, X. Chen, W. Liu, J. Yu, G. Yu, and T. Chen, "Motiongpt: Human motion as a foreign language," in *NeurIPS*, 2024.
- [300] Y. Zhang, D. Huang, B. Liu, S. Tang, Y. Lu, L. Chen, L. Bai, Q. Chu, N. Yu, and W. Ouyang, "Motiongpt: Finetuned llms are general-purpose motion generators," in *AAAI*, 2024, pp. 7368–7376.
- [301] C. Guo, Y. Mu, M. G. Javed, S. Wang, and L. Cheng, "Momask: Generative masked modeling of 3d human motions," in *CVPR*, 2024, pp. 1900–1910.
- [302] G. Tevet, S. Raab, B. Gordon, Y. Shafir, D. Cohen-Or, and A. H. Bermano, "Human motion diffusion model," in *ICLR*, 2022.
- [303] R. Dabral, M. H. Mughal, V. Golyanik, and C. Theobalt, "Mofusion: A framework for denoising-diffusion-based motion synthesis," in *CVPR*, 2023, pp. 9760–9770.
- [304] Y. Yuan, J. Song, U. Iqbal, A. Vahdat, and J. Kautz, "Physdiff: Physics-guided human motion diffusion model," in *ICCV*, 2023, pp. 16010–16021.
- [305] M. Zhang, X. Guo, L. Pan, Z. Cai, F. Hong, H. Li, L. Yang, and Z. Liu, "Remodiffuse: Retrieval-augmented motion diffusion model," in *ICCV*, 2023.
- [306] Y. Bian, A. Zeng, X. Ju, X. Liu, Z. Zhang, W. Liu, and Q. Xu, "Motioncraft: Crafting whole-body motion with plug-and-play multimodal controls," *arXiv*, 2024.
- [307] X. Liu, J. Ren, A. Siarohin, I. Skorokhodov, Y. Li, D. Lin, X. Liu, Z. Liu, and S. Tulyakov, "Hyperhuman: Hyper-realistic human generation with latent structural diffusion," *arXiv*, 2023.
- [308] F. Hong, M. Zhang, L. Pan, Z. Cai, L. Yang, and Z. Liu, "Avatarclip: Zero-shot text-driven generation and animation of 3d avatars," *SIGGRAPH*, 2022.
- [309] C. Guo, X. Zuo, S. Wang, and L. Cheng, "Tm2t: Stochastic and tokenized modeling for the reciprocal generation of 3d human motions and texts," in *ECCV*, 2022, pp. 580–597.
- [310] Y. Xie, V. Jampani, L. Zhong, D. Sun, and H. Jiang, "Omnicontrol: Control any joint at any time for human motion generation," in *ICLR*, 2024.
- [311] J. Liu, W. Dai, C. Wang, Y. Cheng, Y. Tang, and X. Tong, "Plan, posture and go: Towards open-world text-to-motion generation," *ECCV*, 2024.
- [312] W. Zhou, Z. Dou, Z. Cao, Z. Liao, J. Wang, W. Wang, Y. Liu, T. Komura, W. Wang, and L. Liu, "Emdm: Efficient motion diffusion model for fast, high-quality motion generation," *ECCV*, 2024.
- [313] M. Petrovich, O. Litany, U. Iqbal, M. J. Black, G. Varol, X. Bin Peng, and D. Remppe, "Multi-track timeline control for text-driven 3d human motion generation," in *CVPRW*, 2024, pp. 1911–1921.
- [314] B. Li, Y. Zhao, S. Zhelun, and L. Sheng, "Danceformer: Music conditioned 3d dance generation with parametric motion transformer," in *AAAI*, 2022, pp. 1272–1279.
- [315] L. Siyao, W. Yu, T. Gu, C. Lin, Q. Wang, C. Qian, C. C. Loy, and Z. Liu, "Bailando: 3d dance generation by actor-critic gpt with choreographic memory," in *CVPR*, 2022, pp. 11050–11059.
- [316] J. Tseng, R. Castellon, and K. Liu, "Edge: Editable dance generation from music," in *CVPR*, 2023, pp. 448–458.
- [317] R. Li, Y. Zhang, Y. Zhang, H. Zhang, J. Guo, Y. Zhang, Y. Liu, and X. Li, "Lodge: A coarse to fine diffusion network for long dance generation guided by the characteristic dance primitives," in *CVPR*, 2024, pp. 1524–1534.